

Recent advances in physiologically based pharmacokinetic and pharmacodynamic models for anticancer nanomedicines

Jong Hyuk Byun¹ · Dong-Gyun Han² ·
Hyun-Jong Cho³  · In-Soo Yoon² · Il Hyo Jung¹

Received: 3 October 2019 / Accepted: 9 January 2020 / Published online: 23 January 2020
© The Pharmaceutical Society of Korea 2020

Abstract Nanoparticles (NPs) have distinct pharmacokinetic (PK) properties and can potentially improve the absorption, distribution, metabolism, and elimination (ADME) of small-molecule drugs loaded therein. Owing to the unwanted toxicities of anticancer agents in healthy organs and tissues, their precise delivery to the tumor is an essential requirement. There have been numerous advancements in the development of nanomedicines for cancer therapy. Physiologically based PK (PBPK) models serve as excellent tools for describing and predicting the ADME properties and the efficacy and toxicity of drugs, in combination with pharmacodynamic (PD) models. The recent preliminary application of these modeling approaches to NPs demonstrated their potential benefits in research and development processes relevant to the ADME and pharmacodynamics of NPs and nanomedicines. Here, we comprehensively review the pharmacokinetics of NPs, the developed

PBPK models for anticancer NPs, and the developed PD model for anticancer agents.

Keywords Nanoparticles · Anticancer · PBPK model · PD model · ADME

Introduction

There has been a recent advancement in the development of nanomedicines for cancer therapy (Choi and Han 2018; Hong and Choi 2018; Hwang et al. 2018; Le et al. 2018; Dadfar et al. 2019; Dhandapani et al. 2019; Fu et al. 2019; Gu et al. 2019; Jeon and Ko 2019; Lee 2019; Piao et al. 2019; Qian et al. 2019; Sang et al. 2019; Xiang and Chen 2019; Yoon et al. 2019; Zhang et al. 2019). Owing to the undesirable toxicity of anticancer agents to the healthy organs and tissues, the precise delivery of anticancer drugs to the tumor is an essential requirement. Tumors generally have leaky vasculatures and impaired lymphatic systems. Therefore, macromolecules or particles with higher molecular weights or having a particle diameter higher than the desired cut-off values can evade renal clearance and may be transported to the interstitial space of the tumor. The accumulation of such particles or macromolecules in the tumor is known as the “enhanced permeability and retention (EPR)” effect (Maeda et al. 2000; Fang et al. 2011). The EPR effect has been widely used as a passive tumor targeting strategy for drug delivery (Maeda 2010; Bae and Park 2011). However, since the EPR effect has intrinsic limitations including insufficient targeting efficiency, active tumor targeting strategies, primarily based on ligand–receptor interactions, have been adopted for improving the targeting efficiency (Danhier et al. 2010; Lammers et al. 2012).

Jong Hyuk Byun and Dong-Gyun Han have contributed equally to this work.

- ✉ Hyun-Jong Cho
hjcho@kangwon.ac.kr
- ✉ In-Soo Yoon
insoo.yoon@pusan.ac.kr
- ✉ Il Hyo Jung
ilhjung@pusan.ac.kr

¹ Department of Mathematics, College of Natural Sciences, Pusan National University, Busan 46241, Republic of Korea

² Department of Manufacturing Pharmacy, College of Pharmacy, Pusan National University, Busan 46241, Republic of Korea

³ Department of Pharmacy, College of Pharmacy, Kangwon National University, Chuncheon 24341, Republic of Korea

Numerous types of nanomedicines, including nano-sized particles and macromolecule–drug conjugates, have been developed for cancer therapy (Lee and Cho 2018, 2019; Lee et al. 2018; Chen et al. 2019; Kim et al. 2019). Liposomes (e.g., Myocet[®], Daunoxome[®], and Doxil[®]), polymers (e.g., Oncaspar[®]), polymeric micelles (e.g., Genexol-PM[®]), protein-based nanoparticles (NPs; e.g., Abraxane[®]), and engineered protein (e.g., Ontak[®]) have been clinically approved, while several other diverse candidates are currently in the clinical phase (Lammers et al. 2012). In fact, numerous diverse organic and inorganic material-based nanocarriers have been designed for the delivery of small chemicals, peptides, proteins, and nucleic acids to the tumor (Petros and DeSimone 2010; Pereira et al. 2017; He et al. 2019; Kim et al. 2019; Lee et al. 2019). However, only a few of these are in the clinical phase or are clinically approved. The safety and efficacy of the developed nanomedicines should be sufficiently guaranteed prior to its introduction to the clinical phase or clinical application.

Compared to intact free drugs, nanomedicines can exhibit new efficacy and toxicity issues, because the pharmacokinetic (PK) properties of active pharmaceutical ingredient (API) can be altered upon loading in NP formulations (Yuan et al. 2019). For instance, pegylated liposomal doxorubicin (DOX, Doxil[®]) reduces the clearance mediated by reticuloendothelial system (RES), resulting in a marked increase in the exposure of the plasma and skin to DOX, compared to the exposure observed after the administration of free DOX (Gabizon et al. 2003). Owing to its cutaneous toxicity, the maximal tolerated dose of Doxil[®] (50 mg/m² every 4 weeks) is lower than that of free DOX (60 mg/m² every 3 weeks) (Vail et al. 1998). Furthermore, the accumulation and toxicity of the NPs themselves and their excipients need to be determined. It is crucial to describe and predict the altered PKs, exposure–efficacy relationships, and unintended toxicities during the development and clinical use of nanomedicines.

Physiologically based PK (PBPK) models are mathematical and mechanistic models that are built on the basis of the anatomical and physiological features of the human body and the physicochemical properties of the drugs during the complicated processes of absorption, distribution, metabolism, and excretion (ADME; Nestorov 2003). A PBPK model separates the entire body into individual organ compartments (as building blocks) which are connected to each other by the circulatory system including the blood and lymph (Jones and Rowland-Yeo 2013). PBPK models can predict the mass-time profiles of drugs in individual organs, incorporate the different factors responsible for PK variability, and allow interspecies extrapolation (Nestorov 2007). This model has been accepted by several regulatory agencies, including US Food and Drug Administration (FDA) and European Medicines Agency (EMA), for

various drugs (Sager et al. 2015; Yoshida et al. 2017), and has also been attracting attention as a promising quantitative tool for the assessment and regulation of nano-hazards (Seaton et al. 2010). Furthermore, PBPK models can be used to predict drug efficacy and toxicity when combined with pharmacodynamic (PD) models that relate drug exposure at the site of action to its pharmacological effects (Jones and Rowland-Yeo 2013). This article comprehensively reviews the pharmacokinetics of NPs, the developed PBPK models for anticancer drug-loaded NPs, and the PD models for anticancer agents (Table 1).

Pharmacokinetics of NPs

When administered via extravascular routes, NPs can encounter presystemic clearance mechanisms including chemical/enzymatic degradation and direct removal via excreta such as the feces in oral dosing. The degradation of NPs at the dosing site can result in the release of the loaded APIs, and the APIs released go through their own disposition pathways (Yuan et al. 2019). The NPs that escape the presystemic clearance mechanisms may enter the systemic circulation after crossing various biological absorption barriers, including the unstirred water layer and the gastrointestinal epithelium in case of oral dosing (Lai et al. 2009). To date, however, most NPs have been investigated and developed for intravenous usage, and thus, this review focuses on the behavior of NPs following absorption. After entering the systemic circulation, the NPs are simultaneously distributed to and eliminated by certain organs and tissues. The processes of distribution and elimination of NPs are shown in Fig. 1.

The roles of organs in the distribution and elimination of NPs

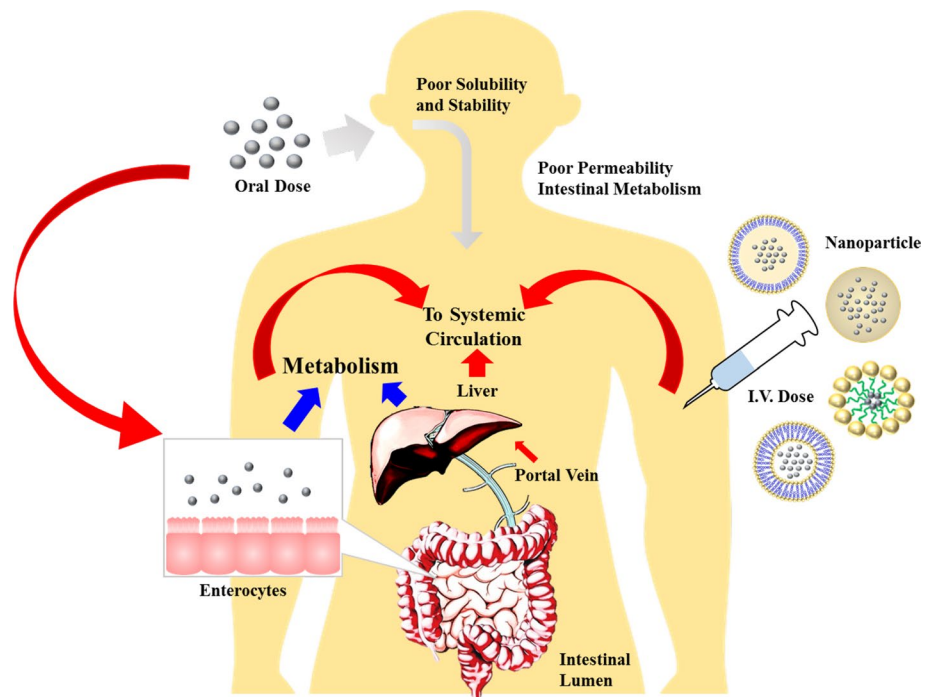
Intravenously administered NPs are first delivered to the lungs by the venous blood flow, and subsequently to the other organs by the arterial blood flow. During this process, each of the organs interacts with the NPs in their own characteristic manner; the NPs can be released, stored, metabolized, and excreted by organs. There are two major routes for the elimination of NPs in the body, the first is the RES, and the second route comprises hepatic metabolism and renal excretion (Wei et al. 2018). The RES, also known as the mononuclear phagocyte system (MPS), mediates phagocytosis and digestion of NPs, followed by excretion of the digested products, which causes a significant loss of the administered dose (von Roemeling et al. 2017). The other elimination route is mediated by the liver and kidney, which function as the major organs for the elimination of NPs. When NPs enter the blood stream, plasma proteins,

Table 1 PD models applied for anticancer agents

General form	Exact model	Drug/target cells	References
$\frac{dT}{dt} = F(T) - G(E, T)$ (2)	$F(T) = k_{in} \left(1 - \frac{T}{TC_{50}+T} \right) T,$ $G(E, T) = k_{in} F \cdot E \cdot T + k_{out} T \text{ or}$ $G(E, T) = E \cdot T + k_{out} T \text{ (8–10)}$	<ul style="list-style-type: none"> • PF06463922 and PF06471402/H3122 (non-small cell lung cancer) cells expressing EML4-ALK • PF02341066/GTL16 (gastric carcinoma) and U87MG (glioblastoma) cells 	Yamazaki et al. (2015, 2008)
	$F(T) = k_{ng} T, G(E, T) = E \cdot T \text{ (11)}$	<ul style="list-style-type: none"> • GDC-0941/MCF7.1 (breast cancer) cells 	Salphati et al. (2010)
	$F(T) = k_{in} \left(1 - \frac{T}{EC_{50}+T} \right) T,$ $G(E, T) = k_{in} F \cdot \frac{I_{max} C}{IC_{50}+C} T \text{ (12)}$	<ul style="list-style-type: none"> • TAK-441/PAN-04 (human pancreatic tumor) cells 	Kogame et al. (2013)
	$F(T) = \frac{k_{ng} T}{\left[1 + \left(\frac{\lambda_0 T}{\lambda_1} \right)^\phi \right]^{\frac{1}{\phi}}},$ $G(T) = F \cdot E \cdot T \text{ (13)}$	<ul style="list-style-type: none"> • LY2157299/Calu6 (non-small cell lung cancer) and MX1 (breast cancer) cells 	Bueno et al. (2008)
$\frac{dT_s}{dt} = F(T_s) - k_{sr} T_s + k_{rs} T_r - G(E, T_s),$ $\frac{dT_r}{dt} = k_{sr} T_s - k_{rs} T_r - k_{deg} T_r \text{ (14)}$	$F(T_s) = k_{ng} T_s,$ $G(E, T_s) = kC \cdot T_s, \frac{E_{max} C^n}{EC_{50}^n + C^n} T_s$ <p>(16)</p> $F(T_s) = kT_s \left(\frac{1-T_s}{T_m} \right), \text{ (16)}$ $G(E, T_s) = kC \cdot T_s \text{ or } \frac{E_{max} C^n}{EC_{50}^n + C^n} T_s$ $F(T_s) = k_{ng} T_s, \text{ (16)}$ $G(E, T_s) = kC \cdot T_s \text{ or } \frac{E_{max} C^n}{EC_{50}^n + C^n} T_s$ $F(T_s) = k_{ng} T_s, G \text{ periodic function}$	<ul style="list-style-type: none"> • Vincristine, vinblastine, arabinosyl-cytosine, and cyclophosphamide/lymphoma and hematopoietic cells • Uracil, Tegafur, and 5-fluorouracil/Colon cancer • Trastuzumab DM1 and brentuximab vedotin/– • Paclitaxel/breast and ovarian cancer 	Jusko (1973) Sung et al. (2009) Vaslaou et al. (2015) Panetta (1997)
$\frac{dT_1}{dt} = F(T_1, T) - G(E, T_1), T_1(0) = T(0),$ $\frac{dT_2}{dt} = G(E, T_1) - \frac{T_2}{\tau}, T_2(0) = 0,$ $\frac{dT_3}{dt} = \frac{1}{\tau} (T_2 - T_3), T_3(0) = 0,$ \vdots $\frac{dT_n}{dt} = \frac{1}{\tau} (T_{n-1} - T_n), T_n(0) = 0,$ $T = \sum_{k=1}^n T_k \text{ (15)}$	$F(T_1, T) = \frac{\lambda_0 T_1}{\left[1 + \left(\frac{\lambda_0 T}{\lambda_1} \right)^\phi \right]^{\frac{1}{\phi}}},$ $G(E, T_1) = kC \cdot T_1 \text{ or } \frac{E_{max} C^n}{EC_{50}^n + C^n} T_1$ <p>(16–17)</p> $F(T_1, T) = k_{ng} T_1^{\frac{2}{3}}$ $G(E, T_1) = \frac{1}{\tau} E T_1^{\frac{2}{3}}$ <p>(16), (18)</p> $F(T_1, T) = \frac{0.693}{DT_{tumor}} T_1$ $G(E, T_1) = \frac{E_{max} Occ_{tub}^n}{EC_{50}^n + Occ_{tub}^n} T_1 \text{ (19–20)}$	<ul style="list-style-type: none"> • Paclitaxel and 5-fluorouracil/A2780 (ovarian carcinoma) and HCT116 (colon carcinoma) cells • Brentuximab vedotin/L540cy (CD30+ Hodgkin's lymphoma) and Karpas 299 (CD30+ anaplastic large cell lymphoma) cells • Novel anticancer candidate/A2780 (ovarian carcinoma) cells • 5-Fluorouracil, cisplatin, docetaxel, doxorubicin, etoposide, gemcitabine, irinotecan, paclitaxel, vinblastine, and vincristine/A2780 (ovarian carcinoma) cells • Aflibercept and DOX/HL-60 (acute myeloid leukemia) and HEL (acute myeloid leukemia)-luciferase cells • Trastuzumab DM1/MMTV-HER2 Fo5 (HER2+ breast cancer) and BT474 EEI (HER2+ breast cancer) cells • Trastuzumab–valine–citrulline–monomethyl auristatin E/N87 (high-HER2) and GFP-MCF7 (low-HER2) tumor 	Simeoni et al. (2004) Shah et al. (2012) Magni et al. (2006) Rocchetti et al. (2007) Fetterly et al. (2013) Jumbe et al. (2010) Singh et al. (2019)

Table 1 (continued)

General form	Exact model	Drug/target cells	References
$\frac{dT}{dt} = F(T) - M_n \cdot G(T), T(0) = T_0,$ $\frac{dM_1}{dt} = \frac{1}{\tau} (E - M_1),$ $\frac{dM_2}{dt} = \frac{1}{\tau} (M_1 - M_2),$ \vdots $\frac{dM_n}{dt} = \frac{1}{\tau} (M_{n-1} - M_n) \quad (21)$	$F(T) = k_{ng} T$ $G(T) = T \quad (11)$	<ul style="list-style-type: none"> • Methotrexate/Ehrlich ascites and sarcoma 180 cells • RG7388/SJSA, RKO, HCT116, H460, A375, SK-MEL-5, SW480, MDA435, and HeLa cells • Doxorubicin and porphyrin-phospholipid (included in liposome)/pancreatic adenocarcinoma 	Lobo and Balthasar (2002) Higgins et al. (2014) Luo et al. (2019)
	$F(T): \text{exponential, logistic, exponential-linear, } G(T) = T$	<ul style="list-style-type: none"> • Paclitaxel/Colon-26 tumor 	Yang et al. (2010)
	$F(T) = k_{ng} T \left(\frac{circ_0}{circ} \right)^{\gamma} \quad (22)$ $G(E, T) = k_{ng} T \cdot E \left(\frac{circ_0}{circ} \right)^{\gamma} + \frac{1}{\tau} T$	<ul style="list-style-type: none"> • Docetaxel, paclitaxel, etoposide, 2'-deoxy-2'-methylidene-cytidine, irinotecan, and vinflunine/leukocyte and neutrophil • Nanoparticle albumin-bound-paclitaxel/neutropenia 	Friberg et al. (2002) Chen et al. (2014)
	$F(T) = 0, G(E, T) = M_2 T \quad (23)$	<ul style="list-style-type: none"> • Free and liposomal doxorubicin/BT4C (rat glioma) and Caki-2 (renal clear cell carcinoma) cells 	Soininen et al. (2016)
	Model switched by time greater than 24 h	<ul style="list-style-type: none"> • Paclitaxel with everolimus and dasatinib/JIMT-1 (HER2+ breast cancer) cells 	Ande et al. (2018)
$\frac{d}{dt}(n(a, t)) = \frac{\partial n}{\partial t} + \frac{\partial n}{\partial a}$ $= -\mu(a, C, T)n, \quad 24$ $n(0, t) = \int_0^{\infty} \lambda(a, c, T)n(a, t) da \quad 25$	The model can be reduced by phase nonspecific model, indirect response models, SDM, CDM, and FDM		Byun and Jung (2019) Belair (1995) Ahmed et al. (2012) Angstmann et al. (2013, 2017)

Fig. 1 Graphical representation of the ADME of intravenously administered NPs

called “opsonins”, and macrophages bind to the surfaces of the NPs, affecting their cellular uptake and clearance (Mirshafiee et al. 2016). The binding of opsonins to NPs results in the formation of dynamic protein coronas, which is called as “opsonization” (Gustafson et al. 2015). The physicochemical characteristics of NPs are therefore altered upon their entry into the systemic circulation (Mahmoudi et al. 2016). The spleen is a part of the MPS, and being structurally similar to a large lymph node, its primary function includes filtering blood (Mebius and Kraal 2005). The nonspecific binding and uptake of NPs can occur in the spleen, primarily in the dense capillary beds and phagocytic regions that are highly abundant in macrophages (Hoshyar et al. 2016). A few studies have reported that nondeformable polymer-decorated NPs of sizes greater than 150 nm are highly likely to get filtered by the spleen (Moghimi et al. 2001, 2005). The major function of the liver involves the metabolism (biotransformation) of xenobiotic substances. The hepatic venous sinus cortex is highly abundant in Kupffer cells that are specialized macrophages with potent phagocytic activity (Helmy et al. 2006), and represents the largest RES in the body. The discontinuous endothelium of sinusoids in the liver allows the transport of NPs from the sinusoids to the hepatocytes, thus enhancing the hepatic distribution and subsequent metabolism of NPs (Wisse et al. 2008; Poisson et al. 2017). Apart from the aforementioned elimination routes, xenobiotic particles can be retained or eliminated by other organs as well. For instance, the boundaries of the pulmonary capillary vessel boundaries can retain xenobiotic particles of sizes greater than 1000 nm during the first pass in the lung following intravenous administration (Moghimi et al. 2012).

Distribution

Following their entry into the systemic circulation, NPs are distributed into various organs and tissues depending on their sizes and interactions with the different components of the body (Sonavane et al. 2008). A previous study suggested that micro-sized metal particles exhibit a longer residence time of approximately two weeks in the spleen compared to that of NPs constituted of the same metal which completely disappeared from the body in the same period (Faraji and Wipf 2009). Generally, gold NPs of larger sizes tend to accumulate in the liver and spleen, while those of smaller sizes tend to accumulate in the kidney (Ravindran et al. 2018). The accumulation of NPs in the tissues also depends on the blood supply to the tissues and the permeability through the vascular endothelium and tissue cells (Li et al. 2010). The effect of the blood supply on the tissue distribution of NPs is determined by comparing the rate of perfused blood flow and the rate of NPs’ transport from the blood into the tissues. When the

blood flow rate is limited, or when the permeation rate into the tissue is rapid, the blood supply can be the rate determining step of NPs’ distribution process (Li et al. 2010). Since the effective pore size in normal endothelium is approximately 5 nm (Choi et al. 2007), NPs of diameter greater than 5 nm barely penetrate the relatively tight vascular endothelium present in organs such as the brain and muscles. NPs of diameter less than 60 nm are more readily distributed into tissues with fenestrated vascular endothelium (existing in gland, kidney, and digestive mucosa with fenestrae of about 60 nm) and into tissues with discontinuous vascular endothelium (existing in spleen, liver, and bone marrow with pores of 50–100 nm) (Yuan et al. 2019). Following their entry into the tissues, NPs may reside in the extracellular matrix, remain attached to the surface of tissue cell, can be transported into the intracellular space, or drained into the lymph nodes (often by transportation mediated by the tissue-resident macrophages) (Longmire et al. 2008; Li et al. 2010).

Numerous NPs have been designed in the past decade for tumor-targeted delivery of small-molecular anticancer and diagnostic agents. NPs can be passively tumor-targeted by the EPR effect, which is closely associated with the abnormal physiological characteristics of tumors, including a limited lymphatic drainage and wide intercellular gaps of 100 to 4700 nm in the vascular endothelium (Greish 2012; Wilhelm et al. 2016). In order to enhance tumor targeting efficiency through the EPR effect, NPs are designed to reside for a prolonged period in blood circulation by avoiding the RES (Li et al. 2010). However, there is no consensus on the optimal size of NPs for ensuring the EPR effect, and it is currently known that the EPR effect is dependent on the stage, type, and size of the tumor (Prabhakar et al. 2013; Perry et al. 2017). Additionally, several factors, including local inflammation, interstitial fibrosis, vessel leakiness, and contraction of the interstitial space, can cause an increase in the interstitial fluid pressure in the tumor, which can be 10- to 40-folds higher than that of normal tissues (Heldin et al. 2004; Yuan et al. 2019). This creates a pressure gradient against the convective transport of NPs from the blood into the tumor, which hinders the EPR effect from working efficiently for NPs (Nichols and Bae 2014). Moreover, NPs can be trapped by the tortuous semisolid extracellular matrix following the extravasation of blood vessels (Taurin et al. 2012; Wilhelm et al. 2016). The NPs in the blood circulation can also be retained and eliminated by other organs of the RES, which generally exhibit a higher uptake capacity than the tumors (Yuan et al. 2019). It is therefore not surprising that the targeting efficiency of NPs, that is the portion of the dose reaching the tumor, reported by previous studies between 2006 and 2016 was estimated to be only 0.7% (median) (Wilhelm et al. 2016). In order to enhance tumor cell uptake, NPs can be actively targeted to the tumor

by decorating them with targeting ligands (i.e., antibody, peptide, or small molecules) which are able to recognize and interact with the cell surface receptors in the tumor (Brannon-Peppas and Blanchette 2004).

Metabolism

The metabolism of NPs is broadly defined as any process that alters the original compositions and/or physicochemical properties of NPs (Li et al. 2010). According to this definition, the decomposition, aggregation, opsonization, and release of the loaded drug fall under NPs' metabolism (Yuan et al. 2019). This review aims to focus on the degradation of NP composites. Depending on their composition, NPs can be uptaken and degraded in the lysosomes of macrophages of RES (Zhang et al. 2016). NPs can also undergo hydrolysis in the aqueous environment of biological systems. Numerous NPs have been prepared with natural polymers (e.g., chitosan and hyaluronic acid), synthetic polymers (e.g., poly(lactic-co-glycolic acid) and poloxamer), and proteins (e.g., albumin). Generally, the degradation rate of natural polymers in biological systems can be faster than that of synthetic polymers (Li et al. 2010). Therefore, the metabolism rate of polymeric NPs can be controlled by the molecular weight and composition of the polymers used (Shive and Anderson 1997). However, various inorganic NPs, prepared with gold, iron oxide, quantum dots, silica, and silver, are known to be very stable and hardly undergo metabolism in the body. Thus, these NPs can persist in the body for a long period of time, potentially leading to their unintended accumulation, which results in NP-associated toxicities (Yang et al. 2007). A previous study reported that polymer-coated quantum dots can remain accumulated in mice over a duration of 2 years (Ballou et al. 2007). The prolonged residence of NPs in macrophages can result in the fusion of macrophages to form dense fibrous capsules (Taurin et al. 2012). A previous study reported the development of sarcoma in rats due to phagocytosis and inflammation associated with cobalt NPs (Hansen et al. 2006). Additionally, the NPs themselves can modulate the functions of the cytochrome P450 (CYP) enzymes that play a major role in the metabolism of most drugs. For instance, a previous study investigating the effect of porous silicon NPs on the activity of four CYP isoforms (CYP1A2/2A6/2D6/3A4) in human liver microsomes reported that the enzymatic activity of CYP2D6 was the most vulnerable to inhibition by the porous silicon NPs, while aminopropylsilane-modified silicon NPs inhibited the activity of CYP2D6 by 80%, which was independent of the NP concentration (Ollikainen et al. 2017). These results can be attributed to the typical enzyme inhibition mechanisms, that is, the competitive, uncompetitive,

and noncompetitive modes of inhibition, the electrostatic interactions of NPs with salts, and/or the nonspecific adsorption of lipids onto the NP surface (Ollikainen et al. 2017).

Excretion

The excretion of NPs refers to the transfer of intact NPs out of the body, which depends on their physicochemical properties (Longmire et al. 2008). It is well known that the kidneys and liver play major roles in the excretion of NPs (Yuan et al. 2019). The renal excretion of NPs are dependent on their size, shape, and surface charge. The kidney glomeruli have three layers, i.e. an endothelium with fenestrae (70–90 nm), glomerular basement membrane (with 2–8 nm pores), and epithelium with filtration slits (4–11 nm). Thus, NPs with a hydrodynamic diameter less than 6 nm can pass through glomerular capillary wall in theory (Liu et al. 2013). Choi et al. reported that > 50% of injected quantum dots with sizes below 5.5 nm can be cleared into the urine 4 h post injection, while quantum dots with the size of 8.65 nm mainly accumulated in the liver (Choi et al. 2007). As the capillary wall of the glomeruli is negatively charged, positively charged NPs with a hydrodynamic diameter of 6–8 nm can pass the kidney filtration barrier, whereas the filtration is difficult for the negatively charged or neutral NPs with the same size (Ohlson et al. 2001; Liu et al. 2013). Additionally, the size is also an important factor for kidney filtration owing to the rectangular shape of the glomerular basement membrane pores. Single walled large linear carbon nanotubes with a rod length of 100–1000 nm and diameter of 0.8–1.2 nm can pass through the kidney with a high efficiency of 65% injected dose excreted in 20 min post injection (Ruggiero et al. 2010). The liver can function as a major organ for the excretion of some NPs. A previous study demonstrated that silica NPs of sizes 50, 100, and 200 nm were excreted in both the urine and bile (Cho et al. 2009). Furumoto and coworkers also reported that polystyrene NPs can be uptaken into both hepatocytes and Kupffer cells, and that approximately 4% of the intravenous dose of NP administered in the study was excreted in the bile in the intact form within 24 h (Furumoto et al. 2001).

PBPK models for anticancer nanomedicines: principles and applications

PBPK models of NPs

Currently, a PBPK model is recognized as a powerful tool for describing and predicting PK properties of chemicals and biologics in pharmaceutical research and development (Zhao et al. 2012; Li et al. 2017). However, the application

of PBPK models to NPs is complicate and challenging owing to several complex factors, including opsonization, EPR effects, RES-mediated clearance, API release kinetics, and changes in the physicochemical properties of NPs, all of which need to be taken into account during modeling (Li et al. 2010). The application of PBPK modeling for studying the ADME of NPs has gained increasing attention in the recent decade. Therefore, studies on the PBPK models are limited in literature; however, some reports provide pertinent aspects for the PBPK models of NPs loaded with anticancer agents. Some examples of the application of PBPK models for the research and development of anticancer nanomedicines are discussed hereafter.

Application to anticancer nanomedicines

The free drug is released from the nanostructures following the administration of nanomedicines. Thus, PBPK modeling for NPs should simultaneously describe the disposition of both the encapsulated drug in NPs and the free (released) drug, together with the in vivo drug release kinetics. Dong and coworkers developed a PBPK model for nanocrystals (< 210 nm) loaded with the anticancer agent SNX-2112 following intravenous administration in rats (Dong et al. 2015). Nanocrystals, also can be regarded as nanosuspensions, are colloidal systems comprising nano-sized pure drug particles dispersed in water, which can be further stabilized by polymers or surfactants (Rabinow 2004; Sudhakar et al. 2014). In the first stage, a whole body PBPK model consisting of liver (li), spleen (sp), intestine (in), lung (lu), kidney (kd), heart (ht), and remainder (rm) (representing all other tissues) was constructed for the nonparticulate drug dissolved in 45% propylene glycol. SNX-2112 was primarily eliminated by the liver (the apparent hepatic clearance, CL_{li}), and the tissue/plasma concentration ratios (K_{pli}) of SNX-2112, plasma flow (Q_{li}) in the heart, intestine, kidney, and spleen were experimentally determined. In the second stage, the PBPK model thus developed for nonparticulate drug was used to construct a PBPK model that additionally incorporated parameters for the nanoparticulate drug in the liver, spleen, and plasma compartment, for distinguishing the nonparticulate (D) from the nanoparticulate (N) drug. The parameters describing the uptake of the nanoparticulate drug into the liver (Up_{li}) and spleen (Up_{sp}) were included in the model for describing the significantly higher uptake of the nanoparticulate drug than the cosolvent formulation. The first-order drug release process was also included in the plasma, liver, and spleen compartment. The model parameters specific for the nanoparticulate drug, including Up_{sp} , Up_{li} , and K_{rel} were estimated by simultaneous fitting to the experimental data. “C” and “V” denote the concentrations of the nonparticulate SNX-2112 and the volume in each

compartment, respectively. “ C^{Nano} ” denotes the concentrations of particulate SNX-2112 in each compartment. The schematic diagram of the PBPK model for the nanoparticulate drug is shown in Fig. 2, and its mass balance equations are provided as below.

$$V_{pl} \frac{dC_{pl}}{dt} = Q_{co} \left[\frac{C_{lu}}{K_{plu}} - C_{pl} \right] + K_{rel} V_{pl} C_{pl}^{Nano},$$

$$V_{pl} \frac{dC_{pl}^{Nano}}{dt} = -K_{rel} V_{pl} C_{pl}^{Nano} - Up_{li} C_{pl}^{Nano} - Up_{sp} C_{pl}^{Nano},$$

$$V_{ht} \frac{dC_{ht}}{dt} = Q_{ht} \left[C_{pl} - \frac{C_{ht}}{K_{pht}} \right],$$

$$V_{sp} \frac{dC_{sp}}{dt} = Q_{sp} \left[C_{pl} - \frac{C_{sp}}{K_{p_{sp}}} \right] + K_{rel} V_{sp} C_{sp}^{Nano},$$

$$V_{sp} \frac{dC_{sp}^{Nano}}{dt} = Up_{sp} C_{pl}^{Nano} - K_{rel} V_{sp} C_{sp}^{Nano},$$

$$V_{in} \frac{dC_{in}}{dt} = Q_{in} \left[C_{pl} - \frac{C_{in}}{K_{pin}} \right],$$

$$V_{rm} \frac{dC_{rm}}{dt} = Q_{rm} \left[C_{pl} - \frac{C_{rm}}{K_{prm}} \right],$$

$$V_{kd} \frac{dC_{kd}}{dt} = Q_{kd} \left[C_{pl} - \frac{C_{kd}}{K_{pkd}} \right],$$

$$V_{li} \frac{dC_{li}}{dt} = Q_{ha} C_{pl} + Q_{in} \frac{C_{in}}{K_{pin}} + Q_{sp} \frac{C_{sp}}{K_{p_{sp}}} - Q_{li} \frac{C_{li}}{K_{pli}} - CL_H C_{li} + K_{rel} V_{li} C_{li}^{Nano},$$

$$V_{li} \frac{dC_{li}^{Nano}}{dt} = Up_{li} C_{pl}^{Nano} - K_{rel} V_{li} C_{li}^{Nano}.$$

Gilkey and coworkers reported the application of the PBPK models for interpreting the biodistribution of fluorescence dye-labeled NPs as a surrogate for dexamethasone-loaded polymeric NPs (< 110 nm) in leukemia therapy (Gilkey et al. 2015). The simulated NP concentration profiles in the spleen, kidney, and liver exhibited initial spikes, whereas those in the plasma declined rapidly, and were consistent with in vivo data previously reported by the group. Notably, the simulation data revealed that

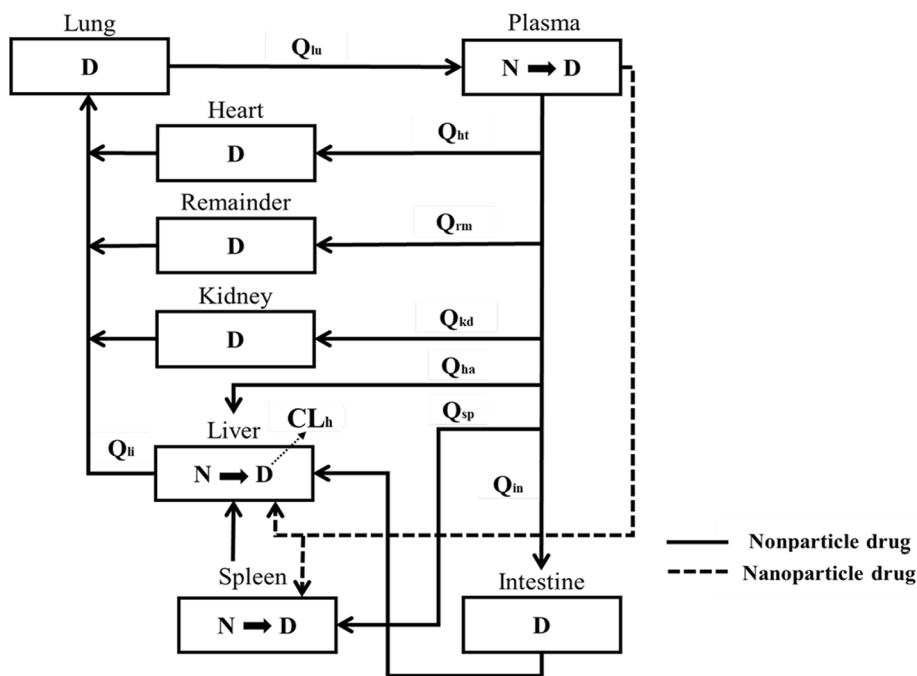


Fig. 2 The whole-body PBPK model for SNX-2112 nanocrystals. Schematic diagram was cited from the literature with slight modification (Dong et al. 2015) and its reuse was approved by the publisher. *ht* heart, *li* liver, *sp* spleen, *lu* lung, *kd* kidney, *in* intestine, *rm* remaining tissues, K_{rel} the first-order rate constant for the release of nonparticulate drug from the nanoparticulate form, Up_{li} , Up_{sp} apparent clearance for NP uptake into the liver and spleen, Q_{ha} the blood flow of the hepatic artery, CL_h hepatic clearance, Q plasma flow, $K_{p,ti}$ tissue/plasma partition coefficient, Q_{ii} plasma flow, V_{ii} organ volume, Q_{co} plasma cardiac output, C concentration of SNX-2112 in each compartment, C , C_{Nano} concentrations of nonparticulate and particulate SNX-2112, respectively, in each compartment

approximately 50% of the injected dose of NPs could be accumulated in the tissues, justifying the inclusion of an additional compartment in the PBPK model. However, the additional compartment that was simultaneously connected to the spleen, kidney, and liver was not physiologically relevant (Li et al. 2017).

Opitz and coworkers developed a PBPK model for describing the biodistribution and elimination of molecular imaging NPs comprising contrast agents and insulin-like growth factor 1 (IGF-1) analogs that were complementary to cancer genes in tumor-bearing mice (Opitz et al. 2010). The NPs exhibited a higher uptake into the tumors than into the surrounding normal tissues. For PBPK modeling, the blood compartment was split into venous and arterial blood compartments, and permeation-limited tissue compartments for the intestine, liver, spleen, lung, heart, kidney, muscle, and tumor were incorporated. The other tissues, including the skin, adipose, brain, and bone, were lumped into one residual compartment. The fitting of the experimentally obtained tissue distribution data to the PBPK model reached convergence only when the dose of NPs bound to the circulating IGF-binding proteins was set to 10–20% of the administered dose. This suggested that the previously reported imaging trials in mice used higher doses of NPs than necessary.

Mager and coworkers reported the application of PBPK modeling for characterizing the biodistribution and elimination of gold/dendrimer composite nanodevices (5 nm and bearing positive/neutral/negative charges, 11 nm and bearing negative charge, and 22 nm and bearing positive charge) in mice with melanoma (Mager et al. 2012). It was assumed that the NPs were exclusively eliminated by biliary and renal excretion in the PBPK model. Furthermore, the permeation-limited tissue compartments were incorporated, similar to the study by Opitz and coworkers. The results of the study demonstrated that the neutral and negatively charged NPs had similar distribution profiles. The PBPK model could also explain the mechanisms of NP elimination by the kidney and RES (especially in the liver and spleen), which varied according to surface charge and particle size. However, no quantitative correlation was found between the charge/size and model parameters.

In addition to the whole-body PBPK models described above, more simplified (hybrid or minimal) PBPK models have also been used, especially for the PK/PD models of anticancer drug-loaded liposomes. The minimal PBPK model is an intermediate concept between the whole-body PBPK and conventional mammillary compartmental models, in which major physiological properties derived from the whole-body PBPK models are lumped (Cao and Jusko

2012). In the PK/PD model proposed by Harashima et al. (1999a, b), the blood compartment was employed as a conventional compartment model for describing the systemic PK properties of liposomal DOX and free DOX. The tumor compartment was divided into capillary, interstitial, and tumor cell sub-compartments, and linked to the blood compartment by tumor blood flow. Drug release, tissue distribution, and intra-tumor disposition were described by the first order rate constants.

Pharmacodynamic models for anticancer agents: theories and applications

Pharmacodynamics is defined as “what the drug does to the body”, and describes the time course of the effects of the drug associated with exposure to response (Lees et al. 2004). Levy and coworkers described pharmacodynamics as the study of the correlation between the effects and drug concentration (Levy 1964). Simulations of PD models can provide information about the optimal dose regimen and various efficacy and safety metrics across all phases. Population pharmacodynamics assesses the profile of the effects of a drug at different concentrations at the population level. These evaluations are performed using the (non-linear) mixed-effect model (Mould and Upton 2013).

Numerous clinical trials have limited sampling due to ethical issues, costs, and reproducibility. Particularly, designing the first-in-human study for anticancer drugs is often more serious than that of other drugs, and should be properly controlled while suppressing the side effects arising from the toxicity of anticancer drugs. Besides, since the therapeutic index of anticancer drugs is narrow, many preclinical studies need to be performed prior to their application in humans. In this regard, a PK/PD model is an efficient and robust support throughout all the phases. According to the guidelines of the FDA for anticancer drugs, the goal of selecting the starting dose is to identify a reasonably safe dose that is expected to have pharmacological effects. PD modeling can also be represented by a well-controlled clinical study that provides substantial evidences regarding the effects of a drug, and which is used to investigate the clinical endpoints and accepted surrogates, or add weight to the evidences supporting the efficacy of the mechanism of action of the drug. PK/PD modeling helps to plan pharmacological response relationships and can explain the differences in the effects of a drug in different nonclinical species (Macheras and Iliadis 2006).

PD models and population PD models have been reviewed in the following sections. It is important to note that tumor size is frequently used as a representative biomarker (Gibbs 2010). We have focused on those models that use continuous PD data, which are derived using PK models from a continuous

drug concentration over time. In this review, the PD models are divided into six categories. The first category comprises the untreated (tumor) growth model, which is developed for systems that are not treated with the drug. The phase non-specific models represent the second category of models. In these models, the effect function for the drug concentration is treated as an independent variable and the drug effect is treated as a dependent variable. In particular, the relationship between the drug concentration and the delay in the effect of the drug is reviewed in greater detail. The third category of models includes the phase-specific models. In these models, the tumor cells are categorized into two types, which are sensitive or resistant to drugs. The cell distribution models (CDMs) represent the fourth category of models, which describe the inhibition of proliferated tumor cells by drugs. The signal distribution models (SDMs) constitute the fifth category of models, which describe the delay in tumor inhibition owing to signal transduction processes. Finally, an age-structured model, which considers the continuous age when drug molecules enter and leave the tumor compartment, is discussed herein.

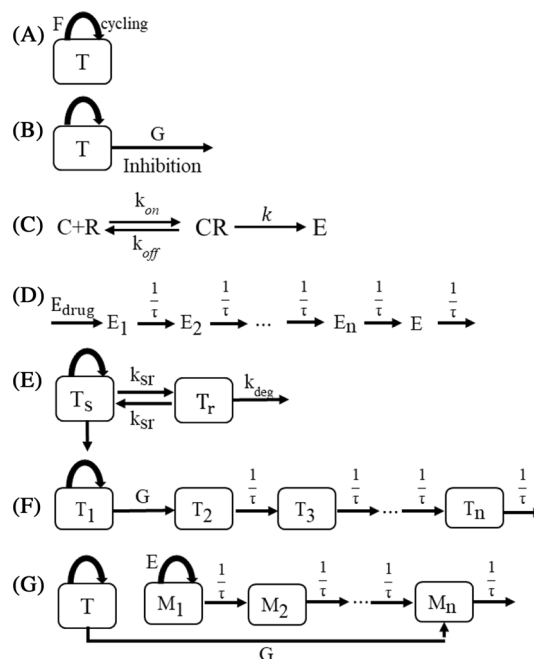


Fig. 3 **a** Phase nonspecific model: growth of tumor cells in the absence of drugs. **b** Inhibition of tumor cells by drug effect function. **c** Drug binds the receptor (R) by mass action law, resulting in the formation of the DR complex. The effect of the drug depends on DR. **d** The response by the transit compartment with a delay in the mean retention time ($1/\tau$) following drug administration. **e** Phase-specific model: tumor cells are categorized as drug-sensitive and drug-resistant. **f** CDM: the total tumor of the tumor cells is expressed as the sum of the number of tumor cells in all the compartments, taking into account that only a fraction of the tumor cells is inhibited by the drug. **g** SDM: the reduction in the number of tumor cells may be delayed by the signal transduction process triggered by the drug

Untreated tumor cell growth models

A tumor cell growth model for systems that are not treated with the drug (Fig. 3a) is represented by

$$\frac{dT}{dt} = F(T), \quad T(0) = T_0, \quad (1)$$

where F represents a family of continuously differentiable functions and is called net growth. As discussed hereafter, the determination of F without linear growth (kT) depends on how rapidly the tumor reaches carrying capacity T_m .

Several models have been constructed by different authors for describing the proliferation of tumor cells. In the most basic model, the tumor cells are considered to grow exponentially. In other words, the rate of change in the number of tumor cells (or sizes) is proportional to the population, and is represented by the following equation:

$$\frac{dT}{dt} = kT,$$

where k represents the first order growth constant. Bissery and coworkers used the exponential model for evaluating growing tumor cells (Bissery et al. 1996). The authors observed that intravenous CPT-11 is highly active against pancreatic ductal adenocarcinoma and was more potent than the other drugs studied therein. Harashima and coworkers developed a physiological model for free DOX and liposomal DOX for clarifying their antitumor efficacy in tumor tissues (Harashima et al. 1999a). They assumed that tumor cells grow exponentially unless the DOX is encapsulated in liposomes. Luo and coworkers described a semi-mechanistic PK-PD model for exploring the antitumor effects of DOX (Luo et al. 2019). The study assumed that pancreatic adenocarcinoma grows exponentially without DOX treatment. Kogame and coworkers used the model for xenograft mice with human pancreatic tumors in the absence of TAK-441 administration (Kogame et al. 2013).

The logistic model assumes that tumor cells grow exponentially; however, tumor growth is limited by the carrying capacity, that is the maximum number of tumor cells owing to the competition for nutrients due to an increased population. The model is represented by the equation:

$$\frac{dT}{dt} = kT \left(1 - \frac{T}{T_m} \right),$$

where T_m represents the carrying capacity. The mathematical interpretation of the model is that the rate of change of $\ln T$ is proportional to the linear function $1 - T/T_m$. Ribba and coworkers have formulated a model for analyzing tumor progression in xenograft nude mice with colorectal adenocarcinoma cells while Spratt and coworkers employed the exponential and the generalized logistic models for fitting

data using least-squares for breast cancer, of which the latter model appeared to be most suitable for fitting the data (Spratt et al. 1993; Ribba et al. 2011). The generalized logistic model is represented by

$$\frac{dT}{dt} = kT \left(1 - \left(\frac{T}{T_m} \right)^N \right), \quad N > 0.$$

The Gompertz model is represented by a sigmoidal curve that fits growth data similar to the logistic model, but is different from the logistic function, in that the two asymptotes are symmetrically approached by the curve. It was originally designed for human mortality but is also applied to the growth of cancer cells. The model is represented by the equation:

$$\frac{dT}{dt} = k \cdot T \cdot \ln \left(\frac{T_m}{T} \right).$$

The first comparison between the model for proliferative tumor cells and the exponential model was provided by Laird (1964). Norton and coworkers used the model to characterize patterns of deviation from normal growth, which appears in response to treatment (Norton and Simon 1977). Barbolosi and coworkers used the model for optimal dosing computations and Tjørve and coworkers first proposed reviewing the existing reparameterizations and models, for discussing their usefulness, and presented a modified form of the Gompertz model (Barbolosi and Iliadis 2001; Tjørve and Tjørve 2017).

The von Bertalanffy model is a generalization of the above equations that can be derived by a suitable assumption (by adjusting a , b , and γ), and is represented by

$$\frac{dT}{dt} = aT^\gamma - bT, \quad \gamma > 0,$$

where γ determines the cellular proliferation. This model assumes that growth is proportional to the surface area, but also considers the decrease in tumor sizes due to cell death (Herman et al. 2011). The value of γ is usually set to $2/3$. Guiot and coworkers explored the growth extension of solid tumor cells, and Herman and coworkers constructed a quantitative and predictive framework for understanding the characteristics of tumor growth and vascularization, which can be viewed as the application of allometric theory to tumor growth modeling (Guiot et al. 2003; Herman et al. 2011). Murphy and coworkers presented the results of various growth models for highlighting the prediction of tumor growth in the presence and absence of chemotherapy (Murphy et al. 2016). When $b=0$, the model is called power-law, which demonstrates that tissue proliferation tissue is proportional to T^γ . In particular, $0 < \gamma < 1$ can be interpreted by fractions of the proliferative tissue. The strategy for

analyzing the tumor growth curve is discussed in detail by Dethlefsen et al. (1968).

The exponential–linear growth model is a combination of the exponential and linear functions and is represented as

$$\frac{dT}{dt} = \lambda_0 T, \quad T(t) \leq T_{th},$$

$$\frac{dT}{dt} = \lambda_1, \quad T(t) > T_{th},$$

where T_{th} represents the threshold tumor size at which growth switching occurs. If $\lambda_0 T_{th} = \lambda_1$, then for a sufficiently large Φ , the system can be simplified as

$$\frac{dT}{dt} = \frac{\lambda_0 T(t)}{\left[1 + \left(\frac{\lambda_0}{\lambda_1} T(t)\right)^\Phi\right]^{\frac{1}{\Phi}}}.$$

Simeoni and coworkers used this model instead of the Gompertz model for focusing on the exponential and linear stages for determining untreated tumor growth in animals (Simeoni et al. 2004). The untreated tumor growth model is also discussed in the study by Benzekry and coworkers (Benzekry et al. 2014).

Drug effect function $E(C)$

The changes in the profiles of tumor size over time can be expressed by tumor growth and inhibition with tumor–drug interactions (Fig. 3b), represented by the following equation:

$$\frac{dT}{dt} = F(T) - G(E, T), \quad (2)$$

where F has been described in Eq. (1) and G represents the drug-induced shrinkage. We also assume that G is a family of continuously differentiable functions. Here, $E = E(C)$ is an effect function which is represented by ratio of the drug effect to the drug concentration C . The concentration–effect relationship for the drug is based on receptor theory (Kenakin 2004), where the drug (C) binds to the receptor (R) resulting in a drug–receptor complex (CR), as shown in Fig. 3c. Here, k_{on} and k_{off} represent the association and dissociation constants, respectively. Additionally, the dissociation rate constant k_D is defined as $k_D = k_{off}/k_{on}$. It therefore follows that $dCR/dt = k_{on}C \cdot R - k_{off}CR$. The theory of chemical equilibrium states that the ratio of R to CR is a function of C and k_D . We can therefore say that $R/CR = k_D/C$ which results in $dCR/dt = 0$. If we define the total receptor by $R_{tot} = CR + R$ and R_{tot} is supposed to constant, then

$$CR = \frac{C \cdot R}{k_D} = \frac{C \cdot (R_{tot} - CR)}{k_D}.$$

It is therefore possible to state that

$$CR = \frac{R_{tot} \cdot C}{k_D + C}.$$

If E is proportional to the CR complex, then

$$E = \frac{E_{max} C}{EC_{50} + C}, \quad (3)$$

where E_{max} represents the maximum concentration, and EC_{50} represents the concentration at which E is 50% of E_{max} . The equation can be revised and generalized:

$$E = \frac{E_{max} C^n}{EC_{50}^n + C^n}, \quad (4)$$

where n represents the number of drug molecules that bind to each receptor. In application, n is mainly used to improve the fit of the data and it is called a sigmoid constant (Upton and Mould 2014). If C is much smaller than EC_{50} , then $E = E_{max} C/EC_{50} = \text{slope} \cdot C$, which leads to a linear concentration effect. If there is a baseline (E_0) in the drug effect, then $E = E_0 \pm E_{drug}$ or $E = E_0(1 \pm E_{drug})$, where

$$E_{drug} = \frac{E_{max} C^n}{EC_{50}^n + C^n} \text{ or } \text{slope} \cdot C. \quad (5)$$

Drug concentration can be also measured at the site of action (within tumor cells) and not in the plasma. In this case, there is the temporal difference between the blood and the site of action (Sheiner et al. 1979), and the concentration of the drug at the target site depends on the PK profile of the drug. Numerous studies have discussed the additive, synergistic, and antagonistic effects of two or more drugs used in combination (Nieuwenhuijs et al. 2003; Bouillon et al. 2004; Friberg et al. 2009; Chang et al. 2011).

Indirect (or turnover) response models are suitable if the delay between drug administration and effect is prolonged (Nagashima et al. 1969; Dayneka et al. 1993; Felmler et al. 2012). The rate of change in the effect function depends on the rate of synthesis (k_{in}) and the rate of degradation (k_{out}) and is represented as:

$$\frac{dE}{dt} = k_{in}(E) - k_{out}(E)E. \quad (6)$$

If both k_{in} and k_{out} are independent of E , Eq. (6) is called a basic response model. There are four types of models describing the stimulated and inhibited rates of synthesis, and the stimulated and inhibited rates of degradation. Therefore, the rates of synthesis and degradation can be represented by $k_{in}(E) = k_{in,0}(1 \pm E_{drug})$ and $k_{out}(E) = k_{out,0}(1 \pm E_{drug})$,

respectively, where E_{drug} is derived from Eq. (5) and $k_{\text{in},0}$ and $k_{\text{out},0}$ are the rate constants. Minami and coworkers used the model for fitting data pertaining to leukopenia treated with paclitaxel (PAC; Minami et al. 1998). Yamazaki and coworkers investigated the inhibition of anaplastic lymphoma kinase (ALK) phosphorylation in tumor cells by fitting the plasma concentrations of ALK inhibitors to the model, along with a hypothetical modulator for accounting for the rebounds observed in ALK (Yamazaki et al. 2015).

The indirect response models can be extended by incorporating additional compartments with the mean retention time ($1/\tau$), as shown in Fig. 3d and are represented as:

$$\frac{dE}{dt} = \frac{1}{\tau}(E_n - E),$$

$$\frac{dE_1}{dt} = E_{\text{drug}} - \frac{1}{\tau}E_1,$$

$$\frac{dE_2}{dt} = \frac{1}{\tau}(E_1 - E_2),$$

⋮

$$\frac{dE_n}{dt} = \frac{1}{\tau}(E_{n-1} - E_n).$$

The model is advantageous when the delay between drug infusion and observable effect is long. Patient leukocyte and neutrophil data obtained after the injection of docetaxel, PAC, and etoposide are used in this model, and the model could fairly describe myelosuppression in a previous study (Friberg et al. 2002). Zamboni and coworkers also compared the PD model of other drugs with immediate effects (Zamboni et al. 2001). When modeling the myelosuppressive effects of anticancer agents, parameters describing the production and destruction of the target cells should be incorporated. PD measurements of chemotherapy-induced neutropenia during the entire treatment cycle can provide important information. In a previous study, a PD model was developed for comparing the temporal course of the neutrophil survival fraction in children to that of nonhuman primates as a potential preclinical model of neutropenia, following the daily administration of topotecan for 5 days at 21 day intervals. The profile of drug response at different concentrations is further discussed somewhere (Mould and Upton 2013).

Phase-specific and nonspecific tumor growth models

Tumor growth inhibition models (TGM) describing tumor inhibition by drugs can be classified as phase-nonspecific or phase-specific models. These models are subdivided

on the basis of the presence or absence of any delay in tumor size inhibition. The phase-specific models, as shown in Fig. 3e, assume that cancer cells are only sensitive to antitumor agents at a certain stage of the cell cycle. These models may include transit compartments to account for the delay between drug administration and tumor inhibition. In contrast, phase-nonspecific models do not generally incorporate transit compartments. Phase-nonspecific models are represented as:

$$\frac{dT}{dt} = F(T) - G(E, T),$$

where $F(T)$ may be an exponential, logistic, Gompertz, von Bertalanffy, power law, or exponential-linear model, as previously discussed. $G(E, T)$ is commonly represented as:

$$G(E, T) = E(t) \cdot T(t), \quad E(t) = \frac{E_{\text{max}} C^n}{EC_{50}^n + C^n}. \quad (7)$$

Yamazaki and coworkers used the model for studying the relationship between c-Met phosphorylation and antitumor efficacy of an anticancer agent (Yamazaki et al. 2008). The TGM of the control group was represented in the study by the following equation:

$$F(T) = k_{\text{in}} \left(1 - \frac{T}{TC_{50} + T} \right) T, \quad (8)$$

and the response of the tumor size to the anticancer agent (PF02341066) followed this equation:

$$\frac{dT}{dt} = k_{\text{in}} \left(1 - \frac{T}{TC_{50} + T} \right) \left(1 - \frac{E_{\text{max}} C^n}{EC_{50}^n + C^n} \right) T - k_{\text{out}} T. \quad (9)$$

In addition, the inhibitor model for ALK was represented (Yamazaki et al. 2015) by:

$$\frac{dT}{dt} = F(T) - E \cdot T - k_{\text{out}} T, \quad (10)$$

where $F(T)$ is used to model logistic or exponential growth. Salphati and coworkers characterized the relationships between the plasma concentration of the anticancer agent GDC-0941 and the reduction in tumor size in a MCF7.1 breast cancer xenograft mouse model (Salphati et al. 2010). The model is represented by the equation:

$$\frac{dT}{dt} = k_{\text{ng}} T - ET, \quad (11)$$

where $E = E(C)$ has been described in Eq. (5). Wong and coworkers used the same model for describing the efficacy of the anticancer agent erlotinib in breast cancer cells in xenograft mice (Wong et al. 2012). Kogame and coworkers explored the possibility of establishing the relationships of

the PK of the anticancer agent TAK-441 with the responses of Gli1 mRNA in tumor-associated stromal or skin cells and with the antitumor effect upon hedgehog inhibition (Kogame et al. 2013). The model is represented by the following equation:

$$\frac{dT}{dt} = k_{in} \left(1 - \frac{T}{EC_{50} + T} \right) \cdot \left(1 - \frac{I_{max}C}{IC_{50} + C} \right) T. \quad (12)$$

The IC_{50} of a drug represents the concentration at which 50% of the maximum inhibition (I_{max}) is achieved. Bueno and coworkers studied the plasma levels of galunisertib, the percentage of pSmad in tumor cells, and the tumor size, for establishing a PD model represented by the equation (Bueno et al. 2008):

$$\frac{dT}{dt} = \frac{k_{ng}(1 - E)T}{\left[1 + \left(\frac{\lambda_0 T}{\lambda_1} \right)^\Phi \right]^{\frac{1}{\Phi}}}, \quad (13)$$

where E represents the indirect response. A two-compartment model was used to account for the signal transduction of pSmad that provides the signal for inhibitory growth.

In the phase-specific model, as shown in Fig. 3e, T_s and T_r represent the drug-sensitive and drug-resistant tumor cells, respectively. If k_{deg} represents the rate of cell death and k_{sr} and k_{rs} indicate rates of cell cycling between populations, then the model is represented as:

$$\frac{dT_s}{dt} = F(T_s) - k_{sr}T_s + k_{rs}T_r - G(T_s, E), \quad (14)$$

$$\frac{dT_r}{dt} = k_{sr}T_s - k_{rs}T_r - k_{deg}T_r.$$

Jusko described the use of this model for analyzing dose–time–cell-survival curves reported by authors studying the effects of vincristine, vinblastine, arabinosylcytosine, and cyclophosphamide on lymphoma and hematopoietic cells in murine femur (Jusko 1973). Sung and coworkers used three PD models, including a phase-specific model for studying the effects of 5-fluorouracil (5-FU) and growth factor F by assuming a logistic growth curve (Sung et al. 2009). Vasalou and coworkers applied a TGM following tumor inhibition by antibody–drug conjugates (ADCs) with the slightly revised model ($k_{deg} = 0$), described by Panetta (Panetta 1997; Vasalou et al. 2015).

CDMs and SDMs

Two models, the CDM, and the SDM, have been developed for describing the delay in tumor shrinkage following drug administration. SDM is also known as the transit compartment model. As shown in Fig. 3f, CDMs, assume that tumor

cells are initially in the proliferative stage, but drug treatment inhibits the proliferation of some tumor cells (Simeoni et al. 2004; Magni et al. 2006). The models identify these inhibited cells by modeling the process of signal transduction. In contrast, SDMs assume that the drug targets the receptor that initiates an effector signal which is transformed through a cascade of transit compartments, as shown in Fig. 3g (Lobo and Balthasar 2002; Yang et al. 2010).

The differential equations of CDM are represented as follows:

$$\frac{dT_1}{dt} = F(T_1, T) - G(E, T_1), \quad T_1(0) = T(0), \quad (15)$$

$$\frac{dT_2}{dt} = G(E, T_1) - \frac{T_2}{\tau}, \quad T_2(0) = 0,$$

$$\frac{dT_3}{dt} = \frac{1}{\tau}(T_2 - T_3), \quad T_3(0) = 0,$$

⋮

$$\frac{dT_n}{dt} = \frac{1}{\tau}(T_{n-1} - T_n), \quad T_n(0) = 0,$$

where the tumor size (T) is the sum of all the compartments, such that $T = \sum_{k=1}^n T_k$. Here, τ represents the mean retention time that is used to describe the transit kinetics. $G(E, T_1)$ is mainly presented by the following equation:

$$G(E, T_1) = kCT_1 \text{ or } \frac{E_{max}C^n}{EC_{50} + C^n}T_1. \quad (16)$$

Simeoni and coworkers used this model for modeling the effect of anticancer agents on tumor growth, which was represented as:

$$F(T_1, T) = \frac{\lambda_0 T_1}{\left[1 + \left(\frac{\lambda_0 T}{\lambda_1} \right)^\Phi \right]^{\frac{1}{\Phi}}}. \quad (17)$$

Shah and coworkers proposed the same growth model for fitting and analyzing data obtained after the administration of brentuximab–vedotine ADC (Simeoni et al. 2004; Shah et al. 2012). Jumbe and coworkers captured the characteristics of tumor growth and the activity of trastuzumab-DM1 ADC (Jumbe et al. 2010), and the resulting model was represented by the following equation:

$$F(T_1, T) = k_{ng}T_1^{\frac{2}{3}} \quad \text{and} \quad G(E, T_1) = \frac{1}{\tau}ET_1^{\frac{2}{3}}. \quad (18)$$

Equation (18) is used for the treatment of spherical tumors, and three compartments are used for measuring the

total tumor size. Magni and coworkers presented a mathematical analysis of the model and suggested an effective strategy for designing *in vivo* experiments in animals, which could save both time and resources (Magni et al. 2006). Rocchetti and coworkers described a method based on a PK/PD model of tumor growth inhibition in xenograft mice, which predicts the parameters for describing the efficacy of the tested compounds (Rocchetti et al. 2007). Fetterly and coworkers discussed the effects of sequential treatment with the potent vascular endothelial growth factor (VEGF) inhibitor (aflibercept; VEGF Trap) and DOX in preclinical acute myeloid leukemia (AML) (Fetterly et al. 2013). PD modeling demonstrated that the observed delay in growth was mainly due to the combination of DOX and VEGF Trap. Singh and coworkers developed an integrated PK/PD model for studying the effect of trastuzumab–valine–citulline–monomethyl auristatin E (T–vc–MMAE) on cells expressing HER2 (Singh et al. 2019). The percent of tubulin occupied by MMAE molecules in the cell is applied to $G(E, T_1)$ instead of MMAE concentration (C). The model is represented by the following equations:

$$F(T_1, T) = \frac{0.693}{DT^{\text{tumor}}} T_1 \quad (19)$$

and

$$G(E, T_1) = \frac{E_{\max} \text{Occ}_{\text{tub}}^n}{EC_{50}^n + \text{Occ}_{\text{tub}}^n} T_1, \quad (20)$$

where Occ_{tub} and DT^{tumor} represent the percentage of occupancy and tumor doubling time, respectively.

The differential equations of SDM are represented as:

$$\frac{dT}{dt} = F(T) - M_n \cdot G(T), \quad (21)$$

$$\frac{dM_1}{dt} = \frac{1}{\tau} (E(C) - M_1),$$

$$\frac{dM_2}{dt} = \frac{1}{\tau} (M_1 - M_2),$$

⋮

$$\frac{dM_n}{dt} = \frac{1}{\tau} (M_{n-1} - M_n),$$

where $E(C)$ has been previously described in Eq. (5). Lobo and coworker investigated the relationship between methotrexate (MTX) exposure and the effects of MTX on tumor cell growth in culture over time, and compared the results with those of a phase-specific model, a nonspecific model, and SDM (Lobo and Balthasar 2002). Yang and coworkers

assessed the usefulness and potential compatibility of CDMs and SDMs (Yang et al. 2010). The results demonstrated that analysis of the simulated tumor response data is more flexible for SDMs on account of the delayed drug effects in tumor volume progression. Higgins and coworkers determined alternative dosing schedules for optimal RG7388-induced antitumor activity based on preclinical data (Higgins et al. 2014). Luo and coworkers used this model for describing the drug-induced tumor shrinkage in laser-treated and non-laser treated groups using long-circulating, sterically stabilized liposomes loaded with DOX in a xenograft mouse model of pancreatic cancer (Luo et al. 2019).

Friberg and coworkers described chemotherapy-induced myelosuppression via drug-specific parameters and system-related parameters (Friberg et al. 2002). A model was developed using patient leukocyte and neutrophil data following the administration of docetaxel, PAC, and etoposide. A feedback mechanism from the circulating cells, expressed as the ratio of baseline concentration of blood cells to the observed concentration of blood cells [represented by $(\text{circ}_0/\text{circ})^\gamma$], was used in this model. The feedback loop was essential for accounting for cellular rebound. The model was represented as:

$$F(T) = k_{\text{ng}} T \left(\frac{\text{circ}_0}{\text{circ}} \right)^\gamma$$

and

$$G(E, T) = k_{\text{ng}} T \cdot E \left(\frac{\text{circ}_0}{\text{circ}} \right)^\gamma + \frac{1}{\tau} T, \quad (22)$$

where $\text{circ} = M_4$, and M_4 has been previously described in Eq. (21). Chen and coworkers characterized a population PK model and the relationship between drug exposure and neutropenia following the administration of NP albumin-bound (nab)-PAC in patients with solid tumors (Chen et al. 2014). Friberg and coworkers described five compartments for neutropenia. Soininen and coworkers discussed that the cellular and nuclear concentrations of DOX were quantifiable with LC/MS following exposure to free and liposomal DOX (pH-sensitive and pegylated liposomes) in rat gliomas and renal clear cell carcinomas (Soininen et al. 2016). A two transit compartment model was selected on the basis of the lowest Akaike information criterion and precision of the parameter estimates. The effect of DOX on cell viability was modeled as:

$$\frac{dT}{dt} = -M_2 T,$$

$$\frac{dM_1}{dt} = \frac{1}{\tau} (E - M_1),$$

$$\frac{dM_2}{dt} = \frac{1}{\tau}(M_1 - M_2), \quad (23)$$

where

$$E = \frac{E_{\max}(C - C_{\text{thr}})}{(EC_{50} - C_{\text{thr}}) + (C - C_{\text{thr}})}.$$

Here C_{thr} represents the threshold nuclear concentration. Threshold concentrations were necessary in the study since the low nuclear concentrations of the drug did not reduce cell viability. Ande and coworkers administered different anticancer agents, including PAC, a mitotic inhibitor combined with everolimus (EVE), an mTOR inhibitor in combination with dasatinib (DAS), and an Src kinase inhibitor, as modalities for overcoming resistance in HER2+ breast cancer (Ande et al. 2018). They used a switch feedback model of the data in a static cell culture setup since all the three drugs appeared daily in the system at the same concentration level.

Age-structured models

The aforementioned models, used discrete compartments for expressing the delay between drug exposure and tumor response, instead of using age as a continuous variable. The age-structured model considers the entry and removal of drug particles from the compartment. The study by M'Kendrick presents the applications of age-structured models for explaining cellular dynamics (M'Kendrick 1925). Drug concentration is interpreted as an environmental factor that affects cell populations and mortality rates. Krzyzanski reviewed an extension of the existing PD models to age-structured models (Krzyzanski 2015). In order to understand the fundamental model, let us consider that $n(a, t)\Delta a$ is the number of tumor cells between the ages of a and $a + \Delta a$ at time t . Then, the total number of cells (T) is defined as $\int_0^\infty n(a, t)da$. The equation describing the relationship between the production of new cells of age 0 and the elimination of aged cells is represented by the equation:

$$\frac{d}{dt}(n(a, t)) = \frac{\partial n}{\partial t} + \frac{\partial n}{\partial a} = -\mu(a, C, T)n, \quad (24)$$

where $\mu(a, C, T)$ represents the rate of cell degradation depending on the age, concentration of drug molecules, and the total number of tumor cells. If age $a=0$, then $n(0, t)$ can be represented by the production of new tumor cells at time t . Therefore,

$$n(0, t) = \int_0^\infty \lambda(a, C, T)n(a, t)da, \quad (25)$$

where $\lambda(a, C, T)$ represents the rate of production of new tumor cells, depending on the age, concentration of drug molecules, and the total number of tumor cells. In application, λ is independent of age a , in which case, $n(0, t) = \lambda(C, T)T^{\text{def}}F(C, T)$. Additionally, μ is independent of the population size and age, that is, $\mu = \mu(C)$. Upon integrating over age a in Eq. (24), the rate of change of T can be described as:

$$\frac{dT}{dt} = F(C, T) - \mu(C)T = F(C, T) - G(C, T).$$

Other models such as CDMs (Krzyzanski 2015) and SDMs (Byun and Jung 2019) can be derived using the gamma distribution. Recently, a fractional-order differential model (FDM) which uses the Mittag-Leffler distribution has been introduced. This is different from the ordinary differential equations in terms of the nonlocal aspects of $d^\alpha T/dt$, $\alpha > 0$. The FDM has been discussed in some related studies (Belair et al. 1995; Ahmed et al. 2012; Angstmann et al. 2013, 2017).

Conclusion

Over the past decade, numerous studies have been conducted for the application of nanotechnology for the diagnosis and treatment of cancer. Nanomedicines can offer several PK advantages over small- and macro-molecular drugs, including improved metabolic stability, enhanced distribution to target tissue, prolonged half-life, and improved bioavailability. Currently, PBPK models are regarded as powerful tools for capturing the complex interplays between drugs and biological systems, and are being increasingly used by regulatory agencies and the pharmaceutical industry. As discussed in this review, a few studies have successfully developed PBPK models that are able to differentiate the behavior of the free drug from the drug entrapped in NPs with incorporating the drug release kinetics. Furthermore, PBPK models for NPs can be coupled with PD models for anticancer agents, which address the temporal profiles of the pharmacological effects of anticancer nanomedicines. However, the application of PBPK modeling to nanomedicines may be limited by the complexity of the disposition of NPs, which includes bio-corona formation (opsonization), particle aggregation, interpatient variability in the bodily response to NPs, and NP heterogeneity. Despite these challenges, PBPK and PD modeling for anticancer nanomedicines remains an emerging field of research that is still in an infant stage. Therefore, further collaborative and multidisciplinary studies are necessary for improving the predictability and validity

of PBPK and PD models for the research and development of anticancer nanomedicines.

Acknowledgements This research was supported by the National Research Foundation of Korea (NRF) Grants funded by the Korea Government (MSIT) (NRF-2019R1A2C2007249).

Compliance with ethical standards

Conflict of interest The authors have declared no conflict of interest.

References

- Ahmed E, Hashish A, Rihan FA (2012) On fractional order cancer model. *J Fract Calc Appl* 3:1–6
- Ande A, Vaidya TR, Tran BN, Vicchiarelli M, Brown AN, Ait-Oudhia S (2018) Utility of a novel three-dimensional and dynamic (3DD) cell culture system for PK/PD studies: evaluation of a triple combination therapy at overcoming anti-HER2 treatment resistance in breast cancer. *Front Pharmacol* 9:403. <https://doi.org/10.3389/fphar.2018.00403>
- Angstmann CN, Donnelly IC, Henry BI (2013) Continuous time random walks with reactions forcing and trapping. *Math Model Nat Phenom* 8:17–27. <https://doi.org/10.1051/mmnp/20138202>
- Angstmann CN, Erickson AM, Henry BI, McGann AV, Murray JM, Nichols JA (2017) Fractional order compartment models. *SIAM J Appl Math* 77:430–446. <https://doi.org/10.1137/16M1069249>
- Bae YH, Park K (2011) Targeted drug delivery to tumors: myths, reality and possibility. *J Control Release* 153:198–205. <https://doi.org/10.1016/j.jconrel.2011.06.001>
- Ballou B, Ernst LA, Andreko S, Harper T, Fitzpatrick JA, Waggoner AS, Bruchez MP (2007) Sentinel lymph node imaging using quantum dots in mouse tumor models. *Bioconjug Chem* 18:389–396. <https://doi.org/10.1021/bc060261j>
- Barbolosi D, Iliadis A (2001) Optimizing drug regimens in cancer chemotherapy: a simulation study using a PK–PD model. *Comput Biol Med* 31:157–172. [https://doi.org/10.1016/S0010-4825\(00\)00032-9](https://doi.org/10.1016/S0010-4825(00)00032-9)
- Belair J, Mackey MC, Mahaffy JM (1995) Age-structured and two-delay models for erythropoiesis. *Math Biosci* 128:317–346. [https://doi.org/10.1016/0025-5564\(94\)00078-E](https://doi.org/10.1016/0025-5564(94)00078-E)
- Benzekry S, Lamont C, Beheshti A, Tracz A, Ebos JM, Hlatky L, Hahnfeldt P (2014) Classical mathematical models for description and prediction of experimental tumor growth. *PLoS Comput Biol* 10:e1003800. <https://doi.org/10.1371/journal.pcbi.1003800>
- Bissery MC, Vrignaud P, Lavelle F, Chabot GG (1996) Experimental antitumor activity and pharmacokinetics of the camptothecin analog irinotecan (CPT-11) in mice. *Anticancer Drugs* 7:437–460. <https://doi.org/10.1097/00001813-199606000-00010>
- Bouillon TW, Bruhn J, Radulescu L, Andresen C, Shafer TJ, Cohane C, Shafer SL (2004) Pharmacodynamic interaction between propofol and remifentanyl regarding hypnosis, tolerance of laryngoscopy, bispectral index, and electroencephalographic approximate entropy. *Anesthesiology* 100:1353–1372. <https://doi.org/10.1097/0000542-200406000-00006>
- Brannon-Peppas L, Blanchette JO (2004) Nanoparticle and targeted systems for cancer therapy. *Adv Drug Deliv Rev* 56:1649–1659. <https://doi.org/10.1016/j.addr.2004.02.014>
- Bueno L, De Alwis DP, Pitou C, Yingling J, Lahn M, Glatt S, Troconiz IF (2008) Semi-mechanistic modelling of the tumour growth inhibitory effects of LY2157299, a new type I receptor TGF-beta kinase antagonist, in mice. *Eur J Cancer* 44:142–150. <https://doi.org/10.1016/j.ejca.2007.10.008>
- Byun JH, Jung IH (2019) Modeling to capture bystander-killing effect by released payload in target positive tumor cells. *BMC Cancer* 19:194. <https://doi.org/10.1186/s12885-019-5336-7>
- Cao Y, Jusko WJ (2012) Applications of minimal physiologically-based pharmacokinetic models. *J Pharmacokinet Pharmacodyn* 39:711–723. <https://doi.org/10.1007/s10928-012-9280-2>
- Chang C, Byun W, Lu Y, Jacobsen LK, Badura LL, Sawant-Basak A, Miller E, Liu J, Grimwood S, Wang EQ, Maurer TS (2011) Quantitative PK–PD model-based translational pharmacology of a novel kappa opioid receptor antagonist between rats and humans. *AAPS J* 13:565–575. <https://doi.org/10.1208/s12248-011-9296-3>
- Chen N, Li Y, Ye Y, Palmisano M, Chopra R, Zhou S (2014) Pharmacokinetics and pharmacodynamics of nab-paclitaxel in patients with solid tumors: disposition kinetics and pharmacology distinct from solvent-based paclitaxel. *J Clin Pharmacol* 54:1097–1107. <https://doi.org/10.1002/jcph.304>
- Chen Q, Chen G, Chen J, Shen J, Zhang X, Wang J, Chan A, Gu Z (2019) Bioresponsive protein complex of aPD1 and aCD47 antibodies for enhanced immunotherapy. *Nano Lett* 19:4879–4889. <https://doi.org/10.1021/acs.nanolett.9b00584>
- Cho M, Cho WS, Choi M, Kim SJ, Han BS, Kim SH, Kim HO, Sheen YY, Jeong J (2009) The impact of size on tissue distribution and elimination by single intravenous injection of silica nanoparticles. *Toxicol Lett* 189:177–183. <https://doi.org/10.1016/j.toxlet.2009.04.017>
- Choi YH, Han HK (2018) Nanomedicines: current status and future perspectives in aspect of drug delivery and pharmacokinetics. *J Pharm Investig* 48:43–60. <https://doi.org/10.1007/s40005-017-0370-4>
- Choi HS, Liu W, Misra P, Tanaka E, Zimmer JP, Itty Ipe B, Bawendi MG, Frangioni JV (2007) Renal clearance of quantum dots. *Nat Biotechnol* 25:1165–1170. <https://doi.org/10.1038/nbt1340>
- Dadfar SM, Roemhild K, Drude NI, Von Stillfried S, Knuchel R, Kiessling F, Lammers T (2019) Iron oxide nanoparticles: diagnostic, therapeutic and theranostic applications. *Adv Drug Deliv Rev* 138:302–325. <https://doi.org/10.1016/j.addr.2019.01.005>
- Danhier F, Feron O, Preat V (2010) To exploit the tumor microenvironment: passive and active tumor targeting of nanocarriers for anti-cancer drug delivery. *J Control Release* 148:135–146. <https://doi.org/10.1016/j.jconrel.2010.08.027>
- Dayneka NL, Garg V, Jusko WJ (1993) Comparison of four basic models of indirect pharmacodynamic responses. *J Pharmacokinet Biopharm* 21:457–478. <https://doi.org/10.1007/BF01061691>
- Dethlefsen LA, Prewitt JM, Mendelsohn ML (1968) Analysis of tumor growth curves. *J Natl Cancer Inst* 40:389–405. <https://doi.org/10.1093/jnci/40.2.389>
- Dhandapani R, Sethuraman S, Subramanian A (2019) Nanohybrid-cancer theranostics for tiny tumor clusters. *J Control Release* 299:21–30. <https://doi.org/10.1016/j.jconrel.2019.02.027>
- Dong D, Wang X, Wang H, Zhang X, Wang Y, Wu B (2015) Elucidating the in vivo fate of nanocrystals using a physiologically based pharmacokinetic model: a case study with the anticancer agent SNX-2112. *Int J Nanomed* 10:2521–2535. <https://doi.org/10.2147/IJN.S79734>
- Fang J, Nakamura H, Maeda H (2011) The EPR effect: unique features of tumor blood vessels for drug delivery, factors involved, and limitations and augmentation of the effect. *Adv Drug Deliv Rev* 63:136–151. <https://doi.org/10.1016/j.addr.2010.04.009>
- Faraji AH, Wipf P (2009) Nanoparticles in cellular drug delivery. *Bioorg Med Chem* 17:2950–2962. <https://doi.org/10.1016/j.bmc.2009.02.043>

- Felmlee MA, Morris ME, Mager DE (2012) Mechanism-based pharmacodynamic modeling. *Methods Mol Biol* 929:583–600. https://doi.org/10.1007/978-1-62703-050-2_21
- Fetterly GJ, Aras U, Lal D, Murphy M, Meholic PD, Wang ES (2013) Development of a preclinical PK/PD model to assess antitumor response of a sequential aflibercept and doxorubicin-dosing strategy in acute myeloid leukemia. *AAPS J* 15:662–673. <https://doi.org/10.1208/s12248-013-9480-8>
- Friberg LE, Henningson A, Maas H, Nguyen L, Karlsson MO (2002) Model of chemotherapy-induced myelosuppression with parameter consistency across drugs. *J Clin Oncol* 20:4713–4721. <https://doi.org/10.1200/JCO.2002.02.140>
- Friberg LE, Vermeulen AM, Petersson KJ, Karlsson MO (2009) An agonist–antagonist interaction model for prolactin release following risperidone and paliperidone treatment. *Clin Pharmacol Ther* 85:409–417. <https://doi.org/10.1038/clpt.2008.234>
- Fu LH, Qi C, Hu YR, Lin J, Huang P (2019) Glucose oxidase-instructed multimodal synergistic cancer therapy. *Adv Mater* 31:e1808325. <https://doi.org/10.1002/adma.201808325>
- Furumoto K, Ogawara K, Yoshida M, Takakura Y, Hashida M, Higaki K, Kimura T (2001) Biliary excretion of polystyrene microspheres depends on the type of receptor-mediated uptake in rat liver. *Biochim Biophys Acta* 1526:221–226. [https://doi.org/10.1016/s0304-4165\(01\)00132-5](https://doi.org/10.1016/s0304-4165(01)00132-5)
- Gabizon A, Shmeeda H, Barenholz Y (2003) Pharmacokinetics of pegylated liposomal doxorubicin: review of animal and human studies. *Clin Pharmacokinet* 42:419–436. <https://doi.org/10.2165/00003088-200342050-00002>
- Gibbs JP (2010) Prediction of exposure–response relationships to support first-in-human study design. *AAPS J* 12:750–758. <https://doi.org/10.1208/s12248-010-9236-7>
- Gilkey MJ, Krishnan V, Scheetz L, Jia X, Rajasekaran AK, Dhurjati PS (2015) Physiologically based pharmacokinetic modeling of fluorescently labeled block copolymer nanoparticles for controlled drug delivery in Leukemia therapy. *CPT Pharmacomet Syst Pharmacol* 4:e00013. <https://doi.org/10.1002/psp4.13>
- Greish K (2012) Enhanced permeability and retention effect for selective targeting of anticancer nanomedicine: are we there yet? *Drug Discov Today Technol* 9:e71–e174. <https://doi.org/10.1016/j.ddtec.2011.11.010>
- Gu Z, Zhu S, Yan L, Zhao F, Zhao Y (2019) Graphene-based smart platforms for combined cancer therapy. *Adv Mater* 31:e1800662. <https://doi.org/10.1002/adma.201800662>
- Guiot C, Degioris PG, Delsanto PP, Gabriele P, Deisboeck TS (2003) Does tumor growth follow a “universal law”? *J Theor Biol* 225:147–151. [https://doi.org/10.1016/s0022-5193\(03\)00221-2](https://doi.org/10.1016/s0022-5193(03)00221-2)
- Gustafson HH, Holt-Casper D, Grainger DW, Ghandehari H (2015) Nanoparticle uptake: the phagocyte problem. *Nano Today* 10:487–510. <https://doi.org/10.1016/j.nantod.2015.06.006>
- Hansen T, Clermont G, Alves A, Eloy R, Brochhausen C, Boutrand JP, Gatti AM, Kirkpatrick CJ (2006) Biological tolerance of different materials in bulk and nanoparticulate form in a rat model: sarcoma development by nanoparticles. *J R Soc Interface* 3:767–775. <https://doi.org/10.1098/rsif.2006.0145>
- Harashima H, Iida S, Urakami Y, Tsuchihashi M, Kiwada H (1999a) Optimization of antitumor effect of liposomally encapsulated doxorubicin based on simulations by pharmacokinetic/pharmacodynamic modeling. *J Control Release* 61:93–106. [https://doi.org/10.1016/S0168-3659\(99\)00110-8](https://doi.org/10.1016/S0168-3659(99)00110-8)
- Harashima H, Tsuchihashi M, Iida S, Doi H, Kiwada H (1999b) Pharmacokinetic/pharmacodynamic modeling of antitumor agents encapsulated into liposomes. *Adv Drug Deliv Rev* 40:39–61. [https://doi.org/10.1016/S0169-409X\(99\)00039-3](https://doi.org/10.1016/S0169-409X(99)00039-3)
- He X, Yin F, Wang D, Xiong LH, Kwok RTK, Gao PF, Zhao Z, Lam JWY, Yong KT, Li Z, Tang BZ (2019) AIE featured inorganic–organic core@shell nanoparticles for high-efficiency siRNA delivery and real-time monitoring. *Nano Lett* 19:2272–2279. <https://doi.org/10.1021/acs.nanolett.8b04677>
- Heldin CH, Rubin K, Pietras K, Ostman A (2004) High interstitial fluid pressure—an obstacle in cancer therapy. *Nat Rev Cancer* 4:806–813. <https://doi.org/10.1038/nrc1456>
- Helmy KY, Katschke KJ Jr, Gorgani NN, Kljavin NM, Elliott JM, Diehl L, Scales SJ, Ghilardi N, Van Lookeren CM (2006) CRIG: a macrophage complement receptor required for phagocytosis of circulating pathogens. *Cell* 124:915–927. <https://doi.org/10.1016/j.cell.2005.12.039>
- Herman AB, Savage VM, West GB (2011) A quantitative theory of solid tumor growth, metabolic rate and vascularization. *PLoS ONE* 6:e22973. <https://doi.org/10.1371/journal.pone.0022973>
- Higgins B, Glenn K, Walz A, Tovar C, Filipovic Z, Hussain S, Lee E, Kolinsky K, Tannu S, Adames V, Garrido R, Linn M, Meille C, Heimbrook D, Vassilev L, Packman K (2014) Preclinical optimization of MDM2 antagonist scheduling for cancer treatment by using a model-based approach. *Clin Cancer Res* 20:3742–3752. <https://doi.org/10.1158/1078-0432.CCR-14-0460>
- Hong SH, Choi Y (2018) Mesoporous silica-based nanoplatfoms for the delivery of photodynamic therapy agents. *J Pharm Investig* 48:3–17. <https://doi.org/10.1007/s40005-017-0356-2>
- Hoshyar N, Gray S, Han H, Bao G (2016) The effect of nanoparticle size on in vivo pharmacokinetics and cellular interaction. *Nanomedicine* 11:673–692. <https://doi.org/10.2217/nnm.16.5>
- Hwang HS, Shin H, Han J, Na K (2018) Combination of photodynamic therapy (PDT) and anti-tumor immunity in cancer therapy. *J Pharm Investig* 48:143–151. <https://doi.org/10.1007/s40005-017-0377-x>
- Jeon G, Ko YT (2019) Enhanced photodynamic therapy via photosensitizer-loaded nanoparticles for cancer treatment. *J Pharm Investig* 49:1–8. <https://doi.org/10.1007/s40005-017-0363-3>
- Jones H, Rowland-Yeo K (2013) Basic concepts in physiologically based pharmacokinetic modeling in drug discovery and development. *CPT Pharmacomet Syst Pharmacol* 2:e63. <https://doi.org/10.1038/psp.2013.41>
- Jumbe NL, Xin Y, Leopold DD, Crocker L, Dugger D, Mai E, Sliwowski MX, Fielder PJ, Tibbitts J (2010) Modeling the efficacy of trastuzumab-DM1, an antibody drug conjugate, in mice. *J Pharmacokinet Pharmacodyn* 37:221–242. <https://doi.org/10.1007/s10928-010-9156-2>
- Jusko WJ (1973) A pharmacodynamic model for cell-cycle-specific chemotherapeutic agents. *J Pharmacokinet Biopharm* 1:175–200. <https://doi.org/10.1007/bf01062346>
- Kenakin T (2004) Principles: receptor theory in pharmacology. *Trends Pharmacol Sci* 25:186–192. <https://doi.org/10.1016/j.tips.2004.02.012>
- Kim KT, Lee JY, Kim DD, Yoon IS, Cho HJ (2019) Recent progress in the development of poly(lactic-co-glycolic acid)-based nanostructures for cancer imaging and therapy. *Pharmaceutics* 11:E280. <https://doi.org/10.3390/pharmaceutics11060280>
- Kogame A, Tagawa Y, Shibata S, Tojo H, Miyamoto M, Tohyama K, Kondo T, Prakash S, Shyu WC, Asahi S (2013) Pharmacokinetic and pharmacodynamic modeling of hedgehog inhibitor TAK-441 for the inhibition of Gli1 messenger RNA expression and antitumor efficacy in xenografted tumor model mice. *Drug Metab Dispos* 41:727–734. <https://doi.org/10.1124/dmd.112.049650>
- Krzyzanski W (2015) Pharmacodynamic models of age-structured cell populations. *J Pharmacokinet Pharmacodyn* 42:573–589. <https://doi.org/10.1007/s10928-015-9446-9>
- Lai SK, Wang YY, Hanes J (2009) Mucus-penetrating nanoparticles for drug and gene delivery to mucosal tissues. *Adv Drug Deliv Rev* 61:158–171. <https://doi.org/10.1016/j.addr.2008.11.002>
- Laird AK (1964) Dynamics of tumor growth. *Br J Cancer* 18:490–502. <https://doi.org/10.1038/bjc.1964.55>

- Lammers T, Kiessling F, Hennink WE, Storm G (2012) Drug targeting to tumors: principles, pitfalls and (pre-) clinical progress. *J Control Release* 161:175–187. <https://doi.org/10.1016/j.jconrel.2011.09.063>
- Le QV, Choi J, Oh YK (2018) Nano delivery systems and cancer immunotherapy. *J Pharm Investig* 48:527–539. <https://doi.org/10.1007/s40005-018-0399-z>
- Lee MK (2019) Clinical usefulness of liposomal formulations in cancer therapy: lessons from the experiences of doxorubicin. *J Pharm Investig* 49:203–214. <https://doi.org/10.1007/s40005-018-0398-0>
- Lee SY, Cho HJ (2018) An alpha-tocopheryl succinate enzyme-based nanoassembly for cancer imaging and therapy. *Drug Deliv* 25:738–749. <https://doi.org/10.1080/10717544.2018.1446476>
- Lee SY, Cho HJ (2019) Mitochondria targeting and destabilizing hyaluronic acid derivative-based nanoparticles for the delivery of lapatinib to triple-negative breast cancer. *Biomacromol* 20:835–845. <https://doi.org/10.1021/acs.biomac.8b01449>
- Lee SY, Ko SH, Shim JS, Kim DD, Cho HJ (2018) Tumor targeting and lipid rafts disrupting hyaluronic acid-cyclodextrin-based nanoassembled structure for cancer therapy. *ACS Appl Mater Interfaces* 10:36628–36640. <https://doi.org/10.1021/acsam.1i.8b08243>
- Lee YW, Luther DC, Kretzmann JA, Burden A, Jeon T, Zhai S, Rotello VM (2019) Protein delivery into the cell cytosol using non-viral nanocarriers. *Theranostics* 9:3280–3292. <https://doi.org/10.7150/thno.34412>
- Lees P, Cunningham FM, Elliott J (2004) Principles of pharmacodynamics and their applications in veterinary pharmacology. *J Vet Pharmacol Ther* 27:397–414. <https://doi.org/10.1111/j.1365-2885.2004.00620.x>
- Levy G (1964) Relationship between elimination rate of drugs and rate of decline of their pharmacologic effects. *J Pharm Sci* 53:342–343. <https://doi.org/10.1002/jps.2600530325>
- Li M, Al-Jamal KT, Kostarelos K, Reineke J (2010) Physiologically based pharmacokinetic modeling of nanoparticles. *ACS Nano* 4:6303–6317. <https://doi.org/10.1021/nl1018818>
- Li M, Zou P, Tyner K, Lee S (2017) Physiologically based pharmacokinetic (PBPK) modeling of pharmaceutical nanoparticles. *AAPS J* 19:26–42. <https://doi.org/10.1208/s12248-016-0010-3>
- Liu J, Yu M, Zhou C, Zheng J (2013) Renal clearable inorganic nanoparticles: a new frontier of bionanotechnology. *Mater Today* 16:477–486. <https://doi.org/10.1016/j.mattod.2013.11.003>
- Lobo ED, Balthasar JP (2002) Pharmacodynamic modeling of chemotherapeutic effects: application of a transit compartment model to characterize methotrexate effects in vitro. *AAPS PharmSciTech* 4:E42. <https://doi.org/10.1208/ps040442>
- Longmire M, Choyke PL, Kobayashi H (2008) Clearance properties of nano-sized particles and molecules as imaging agents: considerations and caveats. *Nanomedicine* 3:703–717. <https://doi.org/10.2217/17435889.3.5.703>
- Luo D, Carter KA, EaG M, Straubinger NL, Geng J, Shao S, Jusko WJ, Straubinger RM, Lovell JF (2019) Pharmacokinetics and pharmacodynamics of liposomal chemophototherapy with short drug-light intervals. *J Control Release* 297:39–47. <https://doi.org/10.1016/j.jconrel.2019.01.030>
- Macheras P, Iliadis A (2006) Modeling in biopharmaceutics, pharmacokinetics, and pharmacodynamics. *Interdiscip Appl Math* 30:3–14. <https://doi.org/10.1007/978-3-319-27598-7>
- Maeda H (2010) Tumor-selective delivery of macromolecular drugs via the EPR effect: background and future prospects. *Bioconjug Chem* 21:797–802. <https://doi.org/10.1021/bc100070g>
- Maeda H, Wu J, Sawa T, Matsumura Y, Hori K (2000) Tumor vascular permeability and the EPR effect in macromolecular therapeutics: a review. *J Control Release* 65:271–284. [https://doi.org/10.1016/S0168-3659\(99\)00248-5](https://doi.org/10.1016/S0168-3659(99)00248-5)
- Mager DE, Mody V, Xu C, Forrest A, Lesniak WG, Nigavekar SS, Kariapper MT, Minc L, Khan MK, Balogh LP (2012) Physiologically based pharmacokinetic model for composite nanodevices: effect of charge and size on in vivo disposition. *Pharm Res* 29:2534–2542. <https://doi.org/10.1007/s11095-012-0784-7>
- Magni P, Simeoni M, Poggesi I, Rocchetti M, De Nicolao G (2006) A mathematical model to study the effects of drugs administration on tumor growth dynamics. *Math Biosci* 200:127–151. <https://doi.org/10.1016/j.mbs.2005.12.028>
- Mahmoudi M, Bertrand N, Zope H, Farokhzad OC (2016) Emerging understanding of the protein corona at the nano-bio interfaces. *Nano Today* 11:817–832. <https://doi.org/10.1016/j.nantod.2016.10.005>
- Mebius RE, Kraal G (2005) Structure and function of the spleen. *Nat Rev Immunol* 5:606–616. <https://doi.org/10.1038/nri1669>
- Minami H, Sasaki Y, Saijo N, Ohtsu T, Fujii H, Igarashi T, Itoh K (1998) Indirect-response model for the time course of leukopenia with anticancer drugs. *Clin Pharmacol Ther* 64:511–521. [https://doi.org/10.1016/S0009-9236\(98\)90134-5](https://doi.org/10.1016/S0009-9236(98)90134-5)
- Mirshafiee V, Kim R, Park S, Mahmoudi M, Kraft ML (2016) Impact of protein pre-coating on the protein corona composition and nanoparticle cellular uptake. *Biomaterials* 75:295–304. <https://doi.org/10.1016/j.biomaterials.2015.10.019>
- M'Kendrick AG (1925) Applications of mathematics to medical problems. *Proc Edinb Math Soc* 44:98–130. <https://doi.org/10.1017/S0013091500034428>
- Moghimi SM, Hunter AC, Murray JC (2001) Long-circulating and target-specific nanoparticles: theory to practice. *Pharmacol Rev* 53:283–318
- Moghimi SM, Hunter AC, Murray JC (2005) Nanomedicine: current status and future prospects. *FASEB J* 19:311–330. <https://doi.org/10.1096/fj.04-2747rev>
- Moghimi SM, Hunter AC, Andresen TL (2012) Factors controlling nanoparticle pharmacokinetics: an integrated analysis and perspective. *Annu Rev Pharmacol Toxicol* 52:481–503. <https://doi.org/10.1146/annurev-pharmtox-010611-134623>
- Mould DR, Upton RN (2013) Basic concepts in population modeling, simulation, and model-based drug development—Part 2: introduction to pharmacokinetic modeling methods. *CPT Pharmacomet Syst Pharmacol* 2:e38. <https://doi.org/10.1038/psp.2013.14>
- Murphy H, Jaafari H, Dobrovolsky HM (2016) Differences in predictions of ODE models of tumor growth: a cautionary example. *BMC Cancer* 16:163. <https://doi.org/10.1186/s12885-016-2164-x>
- Nagashima R, O'Reilly RA, Levy G (1969) Kinetics of pharmacologic effects in man: the anticoagulant action of warfarin. *Clin Pharmacol Ther* 10:22–35. <https://doi.org/10.1002/cpt.196910122>
- Nestorov I (2003) Whole body pharmacokinetic models. *Clin Pharmacokinet* 42:883–908. <https://doi.org/10.2165/00003088-200342100-00002>
- Nestorov I (2007) Whole-body physiologically based pharmacokinetic models. *Expert Opin Drug Metab Toxicol* 3:235–249. <https://doi.org/10.1517/17425255.3.2.235>
- Nichols JW, Bae YH (2014) EPR: evidence and fallacy. *J Control Release* 190:451–464. <https://doi.org/10.1016/j.jconrel.2014.03.057>
- Nieuwenhuijs DJ, Olofsen E, Romberg RR, Sarton E, Ward D, Engbers F, Vuyk J, Mooren R, Teppema LJ, Dahan A (2003) Response surface modeling of remifentanyl-propofol interaction on cardiorespiratory control and bispectral index. *Anesthesiology* 98:312–322. <https://doi.org/10.1097/0000542-200302000-00008>
- Norton L, Simon R (1977) Growth curve of an experimental solid tumor following radiotherapy. *J Natl Cancer Inst* 58:1735–1741. <https://doi.org/10.1093/jnci/58.6.1735>

- Ohlson M, Sorensson J, Haraldsson B (2001) A gel-membrane model of glomerular charge and size selectivity in series. *Am J Physiol Ren Physiol* 280:F396–F405. <https://doi.org/10.1152/ajprenal.2001.280.3.F396>
- Ollikainen E, Liu D, Kallio A, Makila E, Zhang H, Salonen J, Santos HA, Sikanen TM (2017) The impact of porous silicon nanoparticles on human cytochrome P450 metabolism in human liver microsomes in vitro. *Eur J Pharm Sci* 104:124–132. <https://doi.org/10.1016/j.ejps.2017.03.039>
- Opitz AW, Wickstrom E, Thakur ML, Wagner NJ (2010) Physiologically based pharmacokinetics of molecular imaging nanoparticles for mRNA detection determined in tumor-bearing mice. *Oligonucleotides* 20:117–125. <https://doi.org/10.1089/oli.2009.0216>
- Panetta JC (1997) A mathematical model of breast and ovarian cancer treated with paclitaxel. *Math Biosci* 146:89–113. [https://doi.org/10.1016/S0025-5564\(97\)00077-1](https://doi.org/10.1016/S0025-5564(97)00077-1)
- Pereira P, Barreira M, Queiroz JA, Veiga F, Sousa F, Figueiras A (2017) Smart micelleplexes as a new therapeutic approach for RNA delivery. *Expert Opin Drug Deliv* 14:353–371. <https://doi.org/10.1080/17425247.2016.1214567>
- Perry JL, Reuter KG, Luft JC, Pecot CV, Zamboni W, DeSimone JM (2017) Mediating passive tumor accumulation through particle size, tumor type, and location. *Nano Lett* 17:2879–2886. <https://doi.org/10.1021/acs.nanolett.7b00021>
- Petros RA, DeSimone JM (2010) Strategies in the design of nanoparticles for therapeutic applications. *Nat Rev Drug Discov* 9:615–627. <https://doi.org/10.1038/nrd2591>
- Piao X, Yin H, Guo S, Wang H, Guo P (2019) RNA nanotechnology to solubilize hydrophobic antitumor drug for targeted delivery. *Adv Sci* 6:1900951. <https://doi.org/10.1002/adv.201900951>
- Poisson J, Lemoine S, Boulanger C, Durand F, Moreau R, Valla D, Rautou PE (2017) Liver sinusoidal endothelial cells: physiology and role in liver diseases. *J Hepatol* 66:212–227. <https://doi.org/10.1016/j.jhep.2016.07.009>
- Prabhakar U, Maeda H, Jain RK, Sevick-Muraca EM, Zamboni W, Farokhzad OC, Barry ST, Gabizon A, Grodzinski P, Blakey DC (2013) Challenges and key considerations of the enhanced permeability and retention effect for nanomedicine drug delivery in oncology. *Cancer Res* 73:2412–2417. <https://doi.org/10.1158/0008-5472.CAN-12-4561>
- Qian X, Zhang J, Gu Z, Chen Y (2019) Nanocatalysts-augmented Fenton chemical reaction for nanocatalytic tumor therapy. *Biomaterials* 211:1–13. <https://doi.org/10.1016/j.biomaterials.2019.04.023>
- Rabinow BE (2004) Nanosuspensions in drug delivery. *Nat Rev Drug Discov* 3:785–796. <https://doi.org/10.1038/nrd1494>
- Ravindran S, Suthar JK, Rokade R, Deshpande P, Singh P, Pratindhi A, Khambadkhar R, Utekar S (2018) Pharmacokinetics, metabolism, distribution and permeability of nanomedicine. *Curr Drug Metab* 19:327–334. <https://doi.org/10.2174/1389200219666180305154119>
- Ribba B, Watkin E, Tod M, Girard P, Grenier E, You B, Giraudo E, Freyer G (2011) A model of vascular tumour growth in mice combining longitudinal tumour size data with histological biomarkers. *Eur J Cancer* 47:479–490. <https://doi.org/10.1016/j.ejca.2010.10.003>
- Rocchetti M, Simeoni M, Pesenti E, De Nicolao G, Poggesi I (2007) Predicting the active doses in humans from animal studies: a novel approach in oncology. *Eur J Cancer* 43:1862–1868. <https://doi.org/10.1016/j.ejca.2007.05.011>
- Ruggiero A, Villa CH, Bander E, Rey DA, Bergkvist M, Batt CA, Manova-Todorova K, Deen WM, Scheinberg DA, Mcdevitt MR (2010) Paradoxical glomerular filtration of carbon nanotubes. *Proc Natl Acad Sci USA* 107:12369–12374. <https://doi.org/10.1073/pnas.0913667107>
- Sager JE, Yu J, Ragueneau-Majlessi I, Isoherranen N (2015) Physiologically based pharmacokinetic (PBPK) modeling and simulation approaches: a systematic review of published models, applications, and model verification. *Drug Metab Dispos* 43:1823–1837. <https://doi.org/10.1124/dmd.115.065920>
- Salphati L, Wong H, Belvin M, Bradford D, Edgar KA, Prior WW, Sampath D, Wallin JJ (2010) Pharmacokinetic–pharmacodynamic modeling of tumor growth inhibition and biomarker modulation by the novel phosphatidylinositol 3-kinase inhibitor GDC-0941. *Drug Metab Dispos* 38:1436–1442. <https://doi.org/10.1124/dmd.110.032912>
- Sang W, Zhang Z, Dai Y, Chen X (2019) Recent advances in nanomaterial-based synergistic combination cancer immunotherapy. *Chem Soc Rev* 48:3771–3810. <https://doi.org/10.1039/c8cs00896e>
- Seaton A, Tran L, Aitken R, Donaldson K (2010) Nanoparticles, human health hazard and regulation. *J R Soc Interface* 7(Suppl 1):S119–S129. <https://doi.org/10.1098/rsif.2009.0252.focus>
- Shah DK, Haddish-Berhane N, Betts A (2012) Bench to bedside translation of antibody drug conjugates using a multiscale mechanistic PK/PD model: a case study with brentuximab-vedotin. *J Pharmacokinetic Pharmacodyn* 39:643–659. <https://doi.org/10.1007/s10928-012-9276-y>
- Sheiner LB, Stanski DR, Vozeh S, Miller RD, Ham J (1979) Simultaneous modeling of pharmacokinetics and pharmacodynamics: application to d-tubocurarine. *Clin Pharmacol Ther* 25:358–371. <https://doi.org/10.1002/cpt.1979253358>
- Shive MS, Anderson JM (1997) Biodegradation and biocompatibility of PLA and PLGA microspheres. *Adv Drug Deliv Rev* 28:5–24. <https://doi.org/10.1016/j.addr.2012.09.004>
- Simeoni M, Magni P, Cammia C, De Nicolao G, Croci V, Pesenti E, Germani M, Poggesi I, Rocchetti M (2004) Predictive pharmacokinetic–pharmacodynamic modeling of tumor growth kinetics in xenograft models after administration of anticancer agents. *Cancer Res* 64:1094–1101. <https://doi.org/10.1158/0008-5472.CAN-03-2524>
- Singh AP, Guo L, Verma A, Wong GG, Shah DK (2019) A cell-level systems PK–PD model to characterize in vivo efficacy of ADCs. *Pharmaceutics* 11:98. <https://doi.org/10.3390/pharmaceutics11020098>
- Soininen SK, Vellonen KS, Heikkinen AT, Auriola S, Ranta VP, Urtti A, Ruponen M (2016) Intracellular PK/PD relationships of free and liposomal doxorubicin: quantitative analyses and PK/PD modeling. *Mol Pharm* 13:1358–1365. <https://doi.org/10.1021/acs.molpharmaceut.6b00008>
- Sonavane G, Tomoda K, Makino K (2008) Biodistribution of colloidal gold nanoparticles after intravenous administration: effect of particle size. *Colloids Surf B* 66:274–280. <https://doi.org/10.1016/j.colsurfb.2008.07.004>
- Spratt JA, Von Fournier D, Spratt JS, Weber EE (1993) Decelerating growth and human breast cancer. *Cancer* 71:2013–2019. [https://doi.org/10.1002/1097-0142\(19930315\)71:6%3c2013:aid-cnrc2820710615%3e3.0.co;2-v](https://doi.org/10.1002/1097-0142(19930315)71:6%3c2013:aid-cnrc2820710615%3e3.0.co;2-v)
- Sudhakar B, Nagajyothi K, Murthy KV (2014) Nanosuspensions as a versatile carrier based drug delivery system—an overview. *Curr Drug Deliv* 11:299–305. <https://doi.org/10.2174/1567201811666140323131342>
- Sung JH, Dhiman A, Shuler ML (2009) A combined pharmacokinetic–pharmacodynamic (PK–PD) model for tumor growth in the rat with UFT administration. *J Pharm Sci* 98:1885–1904. <https://doi.org/10.1002/jps.21536>
- Taurin S, Nehoff H, Greish K (2012) Anticancer nanomedicine and tumor vascular permeability; where is the missing link? *J Control Release* 164:265–275. <https://doi.org/10.1016/j.jconrel.2012.07.013>

- Tjorve KMC, Tjorve E (2017) The use of Gompertz models in growth analyses, and new Gompertz-model approach: an addition to the unified-Richards family. *PLoS ONE* 12:e0178691. <https://doi.org/10.1371/journal.pone.0178691>
- Upton RN, Mould DR (2014) Basic concepts in population modeling, simulation, and model-based drug development: Part 3—introduction to pharmacodynamic modeling methods. *CPT Pharmacomet Syst Pharmacol* 3:e88. <https://doi.org/10.1038/psp.2013.71>
- Vail DM, Chun R, Thamm DH, Garrett LD, Cooley AJ, Obradovich JE (1998) Efficacy of pyridoxine to ameliorate the cutaneous toxicity associated with doxorubicin containing pegylated (stealth) liposomes: a randomized, double-blind clinical trial using a canine model. *Clin Cancer Res* 4:1567–1571
- Vasalou C, Helmlinger G, Gomes B (2015) A mechanistic tumor penetration model to guide antibody drug conjugate design. *PLoS ONE* 10:e0118977. <https://doi.org/10.1371/journal.pone.0118977>
- Von Roemeling C, Jiang W, Chan CK, Weissman IL, Kim BYS (2017) Breaking down the barriers to precision cancer nanomedicine. *Trends Biotechnol* 35:159–171. <https://doi.org/10.1016/j.tibtech.2016.07.006>
- Wei Y, Quan L, Zhou C, Zhan Q (2018) Factors relating to the bio-distribution & clearance of nanoparticles & their effects on in vivo application. *Nanomedicine* 13:1495–1512. <https://doi.org/10.2217/nnm-2018-0040>
- Wilhelm S, Tavares AJ, Dai Q, Ohta S, Audet J, Dvorak HF, Chan WC (2016) Analysis of nanoparticle delivery to tumours. *Nat Rev Mater* 1:16014. <https://doi.org/10.1038/natrevmats.2016.14>
- Wisse E, Jacobs F, Topal B, Frederik P, De Geest B (2008) The size of endothelial fenestrae in human liver sinusoids: implications for hepatocyte-directed gene transfer. *Gene Ther* 15:1193–1199. <https://doi.org/10.1038/gt.2008.60>
- Wong H, Choo EF, Aliche B, Ding X, La H, Mcnamara E, Theil FP, Tibbitts J, Friedman LS, Hop CE, Gould SE (2012) Antitumor activity of targeted and cytotoxic agents in murine subcutaneous tumor models correlates with clinical response. *Clin Cancer Res* 18:3846–3855. <https://doi.org/10.1158/1078-0432.CCR-12-0738>
- Xiang H, Chen Y (2019) Energy-converting nanomedicine. *Small* 15:e1805339. <https://doi.org/10.1002/smll.201805339>
- Yamazaki S, Skaptason J, Romero D, Lee JH, Zou HY, Christensen JG, Koup JR, Smith BJ, Koudriakova T (2008) Pharmacokinetic–pharmacodynamic modeling of biomarker response and tumor growth inhibition to an orally available cMet kinase inhibitor in human tumor xenograft mouse models. *Drug Metab Dispos* 36:1267–1274. <https://doi.org/10.1124/dmd.107.019711>
- Yamazaki S, Lam JL, Zou HY, Wang H, Smeal T, Vicini P (2015) Mechanistic understanding of translational pharmacokinetic–pharmacodynamic relationships in nonclinical tumor models: a case study of orally available novel inhibitors of anaplastic lymphoma kinase. *Drug Metab Dispos* 43:54–62. <https://doi.org/10.1124/dmd.114.061143>
- Yang RS, Chang LW, Wu JP, Tsai MH, Wang HJ, Kuo YC, Yeh TK, Yang CS, Lin P (2007) Persistent tissue kinetics and redistribution of nanoparticles, quantum dot 705, in mice: ICP-MS quantitative assessment. *Environ Health Perspect* 115:1339–1343. <https://doi.org/10.1289/ehp.10290>
- Yang J, Mager DE, Straubinger RM (2010) Comparison of two pharmacodynamic transduction models for the analysis of tumor therapeutic responses in model systems. *AAPS J* 12:1–10. <https://doi.org/10.1208/s12248-009-9155-7>
- Yoon SW, Shin DH, Kim JS (2019) Liposomal itraconazole formulation for the treatment of glioblastoma using inclusion complex with HP- β -CD. *J Pharm Investig* 49:477–483. <https://doi.org/10.1007/s40005-019-00432-4>
- Yoshida K, Budha N, Jin JY (2017) Impact of physiologically based pharmacokinetic models on regulatory reviews and product labels: frequent utilization in the field of oncology. *Clin Pharmacol Ther* 101:597–602. <https://doi.org/10.1002/cpt.622>
- Yuan D, He H, Wu Y, Fan J, Cao Y (2019) Physiologically based pharmacokinetic modeling of nanoparticles. *J Pharm Sci* 108:58–72. <https://doi.org/10.1016/j.xphs.2018.10.037>
- Zamboni WC, D'Argenio DZ, Stewart CF, Macvittie T, Delauter BJ, Farese AM, Potter DM, Kubat NM, Tubergen D, Egorin MJ (2001) Pharmacodynamic model of topotecan-induced time course of neutropenia. *Clin Cancer Res* 7:2301–2308
- Zhang YN, Poon W, Tavares AJ, Mcgilvray ID, Chan WCW (2016) Nanoparticle–liver interactions: cellular uptake and hepatobiliary elimination. *J Control Release* 240:332–348. <https://doi.org/10.1016/j.jconrel.2016.01.020>
- Zhang P, Miska J, Lee-Chang C, Rashidi A, Panek WK, An S, Zannikou M, Lopez-Rosas A, Han Y, Xiao T, Pituch KC, Kanojia D, Balyasnikova IV, Lesniak MS (2019) Therapeutic targeting of tumor-associated myeloid cells synergizes with radiation therapy for glioblastoma. *Proc Natl Acad Sci USA* 116:23714–23723. <https://doi.org/10.1073/pnas.1906346116>
- Zhao P, Rowland M, Huang SM (2012) Best practice in the use of physiologically based pharmacokinetic modeling and simulation to address clinical pharmacology regulatory questions. *Clin Pharmacol Ther* 92:17–20. <https://doi.org/10.1038/clpt.2012.68>

Publisher's Note Springer Nature remains neutral with regard to jurisdictional claims in published maps and institutional affiliations.